

SunQM-3s1: Using 1st order spin-perturbation to solve Schrodinger equation for nLL effect and pre-Sun ball's disk-lyzation

Yi Cao

Ph.D. of biophysics, a citizen scientist of QM.

E-mail: yicaojob@yahoo.com

© All rights reserved

The major part of this work started from Sep. 2015, finished in Dec. 2016.

Abstract

Schrodinger equation has been established and solved for the non-spin Solar QM {N,n} structure model in paper SunQM-3. In current paper, the 1st order spin-perturbation problem has been solved for the spinning Sun's {N,n} QM structure. The result shows that the spin-perturbation causes nLL orbit to have the lowest orbit energy (or highest probability density), and it is named as "nLL effect". This study suggests that the nLL effect is the driving force for the Sun's (and all other celestial bodies') flattening, disk-lyzation, ring formation. It is mass occupancy that determines whether the outer shell of a pre-Sun ball goes to flattening or disk-lyzation. The nL0 effect (which is the companion effect of nLL effect) is the driving force for the bipolar outflow and astronomic jet. Additionally, a central G-force caused spherical spin frame theory is established, and our Sun's reference-spin-frame model is expected to be $\omega_{n\text{-spin}} = \omega_{1\text{-spin}} / n^x$, with $x \approx 3$.

Introduction

Thanks those QM scientists who invented the 1st order perturbation QM theory.

As described in wiki "Solar System": "*as the pre-solar nebula... collapsed, conservation of angular momentum caused it to rotate faster. The centre, where most of the mass collected, became increasingly hotter than the surrounding disc. As the contracting nebula rotated faster, it began to flatten into a protoplanetary disc with a diameter of roughly 200 AU.*" So it was well known that the flattening and disk-lyzation of the pre-Sun ball-like structure was mainly caused by its spinning.

In previous paper SunQM-3^[1], I established a non-spinning solar system's (or pre-Sun's) QM model based on {N,n} QM structure and Schrodinger equation/solution. In current paper SunQM-3s1, I will use the same pre-Sun QM model, except now it is spinning, with spin-period (at equator) = 25.38 days, or $\omega_{\text{spin}} = 2\pi/T = 2.865\text{E-}6$ arc/sec, at Sun's surface {0,2}. Then I will treat the spin of the pre-Sun ball as a small perturbation of non-spin pre-Sun ball {N,n} QM model. So then I am going to solve the 1st order perturbation QM of a spinning pre-Sun ball based on a non-spin pre-Sun ball model.

Note-1: The orbital rotation angular velocity at Sun's surface {0,2} is $6.28\text{E-}4$ arc/s, (using data from paper SunQM-2 table 1, calculated as $v_{\text{orbit}} / r_{\text{orbit}} = 4.37\text{E}+5$ (m/s) / $6.96\text{E}+8$ (m)). So $\omega_{\text{Sun-spin}} / \omega_{\text{Sun-orbit-rotation}} = 2.87\text{E-}6 / 6.28\text{E-}4 = 0.46\%$.

Therefore, I can treat the spin of the pre-Sun ball as a small perturbation of non-spin pre-Sun ball model.

Note-2: For {N,n} QM nomenclature as well as the general notes for {N,n} QM model, please see my paper SnQM-p1 section VII.

Note-3: Microsoft Excel's number format is often used in this paper, for example: $x^2 = x^2$, $3.4\text{E}+12 = 3.4*10^{12}$, $5.6\text{E-}9 = 5.6*10^{-9}$.

I. A central G-force caused spin frame QM ω_n theory, its $|\omega|$ value contour line is spherical shaped, and decreases as r_n increases

In this section, I will develop a reference spin frame which is very different from the classical one.

I-a. The physics meaning of spin frame's ω decreasing with r increasing

From book "The physics of everyday phenomena, a conceptual introduction to physics," by W. Thomas Griffith, 5th ed. 2007, pp152, in Figure 8.16, an ice skater goes into a spin. In action-1, she bring back her arms (so that her hands' $r_1 = 0.25$ m, away from spin axis), and her body has angular velocity ω_1 at $r_1 = 0.25$ m. In action-2, she extend her arms (so that hands' $r_2 = 0.5$ m, away from spin axis), and now her body has angular velocity ω_2 at both $r_1 = 0.5$ m and $r_2 = 0.25$ m. From angular momentum conservation, we know that $\omega_1 > \omega_2$.

Now in action-1 (ω_1 at $r_1 = 0.25$ m), if we want to setup a reference-spin-frame (RefSpnFrm) with ω_1 , this RefSpnFrm at $r_1 = 0.25$ m has angular velocity = ω_1 , what is the RefSpnFrm's angular velocity at $r_2 = 0.5$ m? The Newton physics tell us that it is still ω_1 , but now I am going to challenge it: It should be ω_2 , not ω_1 ! The reason is, you can reverse action-1 and action-2 many times, the hands at $r_2 = 0.5$ m only feel ω_2 , never feel ω_1 ! To extract the physics from this model, in this two-actions spin system, if you choose action-1 as the RefSpnFrm, it is equivalent that you choose ω_1 at $r_1 = 0.25$ m in a RefSpnFrm, then the same RefSpnFrm at $r_2 = 0.5$ m must have ω_2 which slower than that at $r_1 = 0.25$ m. Or, if you choose action-2 as the RefSpnFrm, it is equivalent that you choose ω_2 at $r_2 = 0.5$ m in a RefSpnFrm, then the same RefSpnFrm at $r_1 = 0.25$ m must have ω_1 which faster than that at $r_2 = 0.5$ m. The key I learned from this example is that the (traditional Newton's) abstract RefSpnFrm (without mass distribution history) is not practically useful. Only the RefSpnFrm (which carried its mass distribution history) is practically useful!

Now let's add an action-3. Suppose in both actions-1 & -2, the skater's left foot's $r_1 = 0.25$ m. In action-3, she extended her left leg so that her left foot's $r_2 = 0.5$ m, and now her body has angular velocity ω_2' at both $r_2 = 0.5$ m and $r_1 = 0.25$ m. From angular momentum conservation, we know that $\omega_1 > \omega_2 > \omega_2'$. (Note: a real ice skater will start spinning from slower ω to faster ω , or from action-3, to -2, then to -1. Here I setting $\omega_1 > \omega_2 > \omega_2'$ is try to match numbers to that in pre-Sun's spin frame in the next discussion.)

Now if we choose action-1 as the RefSpnFrm (so ω_1 at $r_1 = 0.25$ m), what is the ω at $r_2 = 0.5$ m? It is ω_2 , or ω_2' ? It depends on what action we are studying. If we study the action-2 relative to action-1, we choose a RefSpnFrm with ω_2 at $r_2 = 0.5$ m, and ω_1 at $r_1 = 0.25$ m. If we study the action-3 relative to action-1, we choose a RefSpnFrm with ω_2' at $r_2 = 0.5$ m, and ω_1 at $r_1 = 0.25$ m. Or if we study the action-3 relative to action-2, we choose a RefSpnFrm with ω_2' at $r_2 = 0.5$ m, and ω_2 at $r_1 = 0.25$ m!

What we learned from this excises is that even when we chosen a RefSpnFrm (e.g., ω_1 at $r_1 = 0.25$ m), the ω of this RefSpnFrm at $r_2 = 0.5$ m is still uncertain. It depends on the mass distribution along r that perpendicular to spin axis. If we know that distribution, then the ω of this RefSpnFrm at $r_2 = 0.5$ m is fixed.

A simplified skater's RefSpnFrm model can be like a series of co-spin-axis hollow cylinders. The most inner one (a cylinder of $r \leq r_1$) has ω_1 , the outside hollow cylinder ($r_1 \leq r \leq r_2$) has ω_2 , and the further outside hollow cylinder ($r_2 \leq r \leq r_3$) has ω_3 , and $\omega_1 > \omega_2 > \omega_3$. The value of ω_2 is depend on the hollow cylinder's moment of inertia ($I = 0.5 * m * (r_1^2 + r_2^2)$). If the mass (m) of the hollow cylinder's I is smaller, then ω_2 value will be smaller, and vise versa.

I-b. The pre-Sun ball's reference-spin-frame (SunSpnFrm) model with $\omega_{n\text{-spin}} = \omega_{1\text{-spin}} / n^{\wedge}x$

Now let's apply this knowledge to the pre-Sun ball's reference-spin-frame (SunSpnFrm) that we are really interested in. Here I summarize the two major characters of SunSpnFrm (after many testing and re-thinking):

1) Based on its point-center-radiated G-force-field and mass-distribution, SunSpnFrm's contour lines of $|\omega_n|$ values are spherical shells shaped, with the inner ω ($= \omega_n$) value always $>$ the outer ω ($= \omega_{n+1}$) value.

2) After some tests, I realized that there is a relationship

$$\omega_{n\text{-spin}} = \omega_{1\text{-spin}} / n^{\wedge}x$$

Eq-1

where x can be any real value between 0 and 4. The actual x value depends on the mass distribution along r_n .

3) In a series of simplified models, x can be any one of these integer numbers $x=0, 1, 2, 3,$ and $4,$

Here are some examples:

Example 1, if $x=0,$ then

$$\omega_{n\text{-spin}} = \omega_{1\text{-spin}} \quad \text{Eq-2}$$

It become a classical RefSpnFrm in which ω is independent of r_n . This does not happen in astronomy physics, because high r_n will produce high ω_n that its $v_{n\text{-spin}}$ will tear apart everything.

Example 2, if we have a constant mass density evenly distributed in a ball, first with radius $= r_1,$ with a ball's angular momentum $L_1 = \omega_1 * I_1 = \omega_1 * (2/5)*m*r_1^2,$ then (for same amount of mass) its radius changed to $r_2 (= r_1 * 2^2 = r_1*4),$ with $L_2 = \omega_2 * I_2 = \omega_2 * (2/5)*m*r_2^2.$ With angular momentum conservation, $L_2 = \omega_2 * (2/5)*m*(r_1*2^2)^2 = \omega_2 * (2/5)*m*r_1^2 * (2^4) = \omega_2*(2^4) * I_1,$ which should conserve and equal to $L_1 = \omega_1 * I_1,$ it gives $\omega_{2\text{-spin}} = \omega_{1\text{-spin}} / 2^4,$ which can be expanded to

$$\omega_{n\text{-spin}} = \omega_{1\text{-spin}} / n^x, \text{ at } x=4. \quad \text{Eq-3}$$

So a constant mass ball decreasing its size from r_n to r_1 (with mass density always evenly distributed), it will have $\omega_{n\text{-spin}} = \omega_{1\text{-spin}} / n^x,$ with $x=4.$ In our pre-Sun ball collapse model each collapse causes $> 99\%$ of mass from $\{N, n=2..6\}$ shell space fly into the $\{N, 1\}$ RF ball, so it is close to a fixed mass ball decreases its r from r_2 to $r_1.$ The major difference is that our pre-Sun ball has a log-log mass distribution relative to $r,$ not a mass density = constant.

Example 3, our planets orbit v_n has a relationship of $v_{n\text{-orbit}} = v_{1\text{-orbit}} / n.$ If SunSpnFrm also has a relationship of $v_{n\text{-spin}} = v_{1\text{-spin}} / n,$ then $\omega_{n\text{-spin}} * r_n = \omega_{1\text{-spin}} r_1 / n,$ $\omega_{n\text{-spin}} = \omega_{1\text{-spin}} (r_1/r_n) / n,$ we obtain $\omega_{n\text{-spin}} = \omega_{1\text{-spin}} / n^3.$ So it gives a SunSpnFrm with

$$\omega_{n\text{-spin}} = \omega_{1\text{-spin}} / n^x, \text{ at } x=3 \quad \text{Eq-4}$$

I believe that our Solar system has a SunSpnFrm with $\omega_{n\text{-spin}} = \omega_{1\text{-spin}} / n^x,$ with x around 3, mainly because this makes spin velocity has the same relationship ($v_{n\text{-spin}} = v_{1\text{-spin}} / n$) as that of orbital velocity.

Example 4, in certain arm region of a galaxy, there is a $v_{n\text{-orbit}} \approx v_{1\text{-orbit}}$ relationship (see wiki "Dark matter"). If $\omega_{n\text{-spin}}$ and $\omega_{n\text{-orbit}}$ are interchangeable, this will result in $v_{n\text{-spin}} = v_{1\text{-spin}},$ $\omega_{n\text{-spin}} * r_n = \omega_{1\text{-spin}} * r_1,$ $\omega_{n\text{-spin}} = \omega_{1\text{-spin}} * (r_1/r_n),$ $\omega_{n\text{-spin}} = \omega_{1\text{-spin}} / n^2.$ So it gives a SunSpnFrm with

$$\omega_{n\text{-spin}} = \omega_{1\text{-spin}} / n^x, \text{ at } x=2 \quad \text{Eq-5}$$

In Table 1 below I listed the possible integers for $x (=0, 1, 2, 3, 4).$ It should cover the whole range of x (real or integer).

Table 1. List of $\omega_{n\text{-spin}} = \omega_{1\text{-spin}} / n^x,$ for $x=0, 1, 2, 3,$ and $4.$

$x=$	$\omega_{n\text{-spin}} = \omega_{1\text{-spin}} / n^x$	comment
0	$\omega_{n\text{-spin}} = \omega_{1\text{-spin}}$	a classical RefSpnFrm in which ω is independent of r_n
1	$\omega_{n\text{-spin}} = \omega_{1\text{-spin}} / n$	
2	$\omega_{n\text{-spin}} = \omega_{1\text{-spin}} / n^2$	match $v_{1\text{-spin}} = v_{n\text{-spin}},$ as in galaxy's arm region.
3	$\omega_{n\text{-spin}} = \omega_{1\text{-spin}} / n^3$	match $v_{1\text{-spin}} = v_{n\text{-spin}} * n$
4	$\omega_{n\text{-spin}} = \omega_{1\text{-spin}} / n^4$	a decreasing size mass ball with $D=\text{cnst}$

In section II-c2, II-c5, II-c6, and II-c7, we will use these relations to calculate the 1st order spin-caused perturbation energy for pre-Sun ball disk-lyzation.

4) A G-forced spin-frame without information of mass distribution along r is not much meaningful in physics! It only provides the information of $\omega_1 > \omega_n$, but can't provide information of x . So in astronomical physics, a G-force spin-frame's effect on r_n has to associate with its historical mass distribution along r (up to r_n)! This is just like that the space and time have to be intertwined (in Einstein's special relativity). **In a spin reference frame, the radius (to the spin axis) and the mass density distribution in r-dimension have to be intertwined!**

5) In paper SunQM-1s1, I modeled Solar system's mass density in space between $\{2,1\}$ to $\{4,6\}$, it is $D = 4.37E+28 / r^{3.28}$ (kg/m^3). In paper SunQM-3 section I-f, I modeled Sun ball's mass density, and find that inside Sun ball, it is $D = 1.26E+23 / r^{2.33}$ (kg/m^3). From my physics sense I believe that our SunSpnFrm is $\omega_{n\text{-spin}} = \omega_{1\text{-spin}} / n^x$, with $x=3.28$ for space between $\{2,1\}$ to $\{4,6\}$, and with $x=2.33$ inside Sun ball. For the same reason, I believe that in the galaxies arm region where $v_{n\text{-orbit}} \approx \text{constant}$, it should have mass density $D = C/r^2$, where C is a constant. However, I still need to figure out how to prove it mathematically.

II. The spin causes pre-Sun ball to disk-lyze as shown by solving the 1st order perturbation problem in the Solar QM $\{N,n\}$ structure

II-a. Define a central G-force Sun-spin-frame for $\{N,1\}$ RF pre-Sun ball, its $|\omega|$ value contour line is spherical shaped, and $|\omega|$ value decreases as r_n increases

After some tests and a longtime thinking, I realized that we need to analyze the disk-lyzation of a pre-Sun-ball in a Solar system's spin frame (SunSpnFrm). Now let us define the SunSpnFrm.

Using the right-hand rule (refer to wiki "right-hand rule, A rotating body"), the Sun spin vector ω_{spin} point to the north (the direction of thumb), its spin defined as eastward (the direction of four fingers). All planets and belts in Solar system are also orbital rotating eastward, with their rotation axis overlapping with Sun's spin axis. So the SunSpnFrm is also defined as in eastward spin.



Figure 1. Define the right-hand rule for the spin of Solar system. Figures are copied from:

https://en.wikipedia.org/wiki/Right-hand_rule#/media/File:Right-hand_grip_rule.svg

<http://davidpratt.info/images/fred2.gif>

The purpose to setup a SunSpnFrm is that we want to study the effect of a $\{N,1\}$ RF pre-Sun ball's spin on its nearby out-space, i.e., the spherical shell space between $\{N,2\}$ to $\{N,6\}$. A classical cylinder shaped spin frame is not going to work for it. A spherical shaped spin frame, inspired by the Earth (where a spinning Earth ball affects its outer atmosphere), is adapted here. For a solid ball (like Earth), its spin angular velocity ω is same everywhere on its surface, from equator to pole. For celestial gas ball, I define a zero order approximation of spinning ball surface: its spinning spherical surface like a solid ball's surface, i.e., its ω_{spin} is same everywhere on its surface from equator to pole. For a pre-Sun ball $\{N,1\}$ RF (remember it is a ball made of almost pure hydrogen gas ~ 5 billion years ago), we apply the zero order approximation to its spin, i.e., its ω_{spin} is same everywhere on its surface from equator to pole.

As mentioned in paper SunQM-3, when $\{N+1,1\}$ RF pre-Sun ball collapsed into $\{N,1\}$ RF pre-Sun ball, $> 99\%$ of mass in shell space between $\{N,2\}$ and $\{N,6\}$ fell into $\{N,1\}$, so according to the law of angular momentum conservation, $\omega(N) > \omega(N+1)$. After applying the zero order approximation of spin, the $\{N,1\}$ RF pre-Sun ball also has same ω_{spin} value

everywhere on its surface from equator to pole. So the SunSpnFrm in space between {N,2} and {N,6} is dominated by the spinning {N,1}RF ball, which has $\omega(N)$, which is $> \omega(N+1)$! After repeating the collapse process, we obtain a SunSpnFrm $\omega(N-3) > \omega(N-2) > \omega(N-1) > \omega(N) > \omega(N+1)$. We can apply the same principle to every n shell within each N super-shell, then we obtain a SunSpnFrm which has a quantized ω_n value, with its $|\omega|$ value contour line is spherical shaped, and $|\omega|$ value decreases as r_n increases.

So any central G-force spin-frame (including SunSpnFrm) can be modeled as a series of concentric spherical shells, each (rigid) shell (at r_n) has a specific ω_{n-spin} value, and this ω_{n-spin} value is same on every position in this (rigid) shell, no matter how close (or how far) this position is from the spin axis! There is a relationship $\omega_{n-spin} = \omega_{1-spin} / n^x$. When $x > 0$, the inner (rigid) spherical shell always spins faster than the outer (rigid) spherical shell. When $x = 0$, $\omega_{n-spin} = \omega_{1-spin}$, so it degenerated back to the classical (cylinder shaped) spin frame. When $x < 0$, the inner (rigid) shell always spins slower than the outer (rigid) shell.

Our Sun-spin-frame has $x > 0$, so its inner (rigid) shell always spin faster than the outer (rigid) shell, Most likely, it also follow the $v_{1-spin} = v_{n-spin} * n$ relationship like $v_{n-orbit}$ does, which means its $x=3$, or $\omega_{n-spin} = \omega_{1-spin} / n^3$.

This ω_{n-spin} model is supported by "recent analysis of SOHO mission data favors a faster rotation rate in the core than in the radiative zone above" (see wiki "Sun"). Also, in García's paper [3], it mentioned that "we obtain better correlations with those having an inner rotation rate in the range three to five times higher than the rest of the radiative region".

II-b. The centrifugal force is the main driving force to disk-lyze the pre-Sun's ball structure.

For a spinning pre-Sun ball {N,n}, let us treat the {N,1}RF as the central ball, and study the movement of an object in spherical space between {N,2} and {N,6}. This immediately bring us to remember that how people studied the atmosphere above the spinning Earth. Using the same treatment, we know that there are two forces we need to concern: Coriolis force (F_{cori}) and centrifugal force (F_{cntfgl}). After studied both forces, I found that it is F_{cntfgl} (not the F_{cori}) that make the main contribution to pre-Sun ball disk-lyzation. So in this paper, I only present how the F_{cntfgl} drives the pre-Sun disk-lyzation in QM analysis.

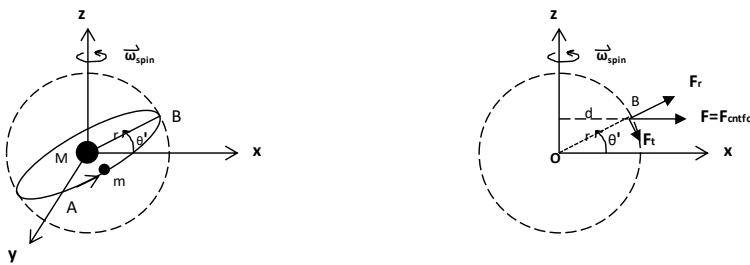


Figure 2. Left: an object m is doing a circular orbit movement around a self-spinning center object M (spin axis along z-axis). Point A $[x,y,z] = [0,r,0]$. Point B $[x,y,z] = [r*cos(\theta'), 0, r*sin(\theta')]$. Point B has the maximum z in the orbit trace. Right: the centrifugal force vector analysis for object m at position B in x-z plane.

Now in our model (as shown in Figure 2-left), the pre-Sun ball {N,1}RF (as shown in M) is spinning along z-axis in angular velocity ω . An arbitrary object (a gas molecule, or a rocky fragment) with a orbital radius r in space between {N,2} and {N,6}, moving in a arbitrary circular orbit. Let us set a coordinate so that its z-axis overlaps pre-Sun ball's spin axis, and the point B (which has the highest z-value in the orbit trace) is in x-z plane. So in this coordinate, the angle between the orbit plane and x-y plane is θ' , Point B $[x,y,z] = [r*cos(\theta'), 0, r*sin(\theta')]$.

Now let us do the force vector analysis at Point B (as shown in Figure 2-right). As described in wiki "Centrifugal force",

$$\mathbf{F}_{\text{cntfgl}} = -m \boldsymbol{\omega}_{\text{spin}} \times (\boldsymbol{\omega}_{\text{spin}} \times \mathbf{d}) \quad \text{Eq-6}$$

where \mathbf{d} is the vertical distance between point B and spin-axis. $d = |\mathbf{d}| = r \cdot \cos(\theta')$. Consider in Schrodinger equation, it only uses θ , and $\theta = \pi/2 - \theta'$. So $d = r \cdot \cos(\pi/2 - \theta)$, or

$$d = r \cdot \sin(\theta) \quad \text{Eq-7}$$

As expected, the centrifugal force always points radial outward from the spin axis, or

$$F_{\text{cntfgl}} = -m \cdot d \cdot \omega_{\text{spin}}^2 \quad \text{Eq-8}$$

Let us decompose the vector $\mathbf{F}_{\text{cntfgl}}$ into F_r in r-direction (or in r-dimension), and F_t in tangential direction (or $\theta\phi$ -2D-dimension, or actually is θ -dimension). F_r in the same r-dimension as gravity force F_g , also $|F_g| \gg |F_t|$. I will analyze the effect of F_r later in section III.

$$F_t = F_{\text{cntfgl}} \cdot \sin(\theta') = F_{\text{cntfgl}} \cdot \cos(\theta) \quad \text{Eq-9}$$

It points to the equator of the SunSpnFrm's spherical shell. Because $F_t > 0$ (comparing to the non-spin SunSpnFrm where $F_t = 0$), even it is not big in value, its relative effect is big. Indeed, as we will see that in the end, this F_t is the major driving force that disk-lyzed the pre-Sun ball.

$$F_t = F_{\text{cntfgl}} \cdot \cos(\theta) = -m \cdot d \cdot \omega_{\text{spin}}^2 \cdot \cos(\theta) = -m \cdot r \cdot \omega_{\text{spin}}^2 \cdot \sin(\theta) \cdot \cos(\theta) \quad \text{Eq-10}$$

The potential energy that F_t generated in the θ -dimension is

$$V_\theta = \int F_t \cdot r \cdot d\theta = \int (-m \cdot r \cdot \omega_{\text{spin}}^2 \cdot \sin(\theta) \cdot \cos(\theta)) \cdot r \cdot d\theta = -m \cdot r^2 \cdot \omega_{\text{spin}}^2 \cdot \int \sin(\theta) \cdot \cos(\theta) \cdot d\theta = (1/2) m \cdot r^2 \cdot \omega_{\text{spin}}^2 \cdot \cos(\theta)^2 \quad \text{Eq-11}$$

or

$$V_\theta = (1/2) m \cdot r^2 \cdot \omega_{\text{spin}}^2 \cdot \cos(\theta)^2 \quad \text{Eq-12}$$

It is obvious that the minimum potential is at $\theta=\pi/2$ where $V_\theta = 0$. Actually in θ -1D-dimension force analysis, the object moves like a pendulum, where F_{cntfgl} is equivalent to F_{gravity} , and both have minimum V at $\theta'=0$. Note: to double check the sign of V_θ : just like that moving to the direction of F_g will get lower V_g , here moving to the direction of F_θ will get lower V_θ , so V_θ has the right sign.

According to section II-a, SunSpnFrm's spherical shell shaped spin ω value decreases as r_n increases, so it should be written as $\omega_{n\text{-spin}}$. So

$$V_\theta = (1/2) m \cdot r_n^2 \cdot \omega_{n\text{-spin}}^2 \cdot \cos(\theta)^2 \quad \text{Eq-13}$$

and at

$$\theta=0, V_\theta = (1/2) m \cdot r_n^2 \cdot \omega_{n\text{-spin}}^2$$

$$\theta=\pi/2, V_\theta = 0$$

$$\theta=\pi, V_\theta = (1/2) m \cdot r_n^2 \cdot \omega_{n\text{-spin}}^2$$

This is a single object (in r_n shell) that has orbit plane angle = θ' and has (the highest z value) B point in z-x plane. In r_n shell of the real pre-Sun ball, there are almost countless objects that have orbit plane angle = θ' , and their (highest z valued) B points form a collection of x-axis that fills all x-y plane (or fill all ϕ -dimension space from 0 to 2π , see more detailed

explanation of RF motion inside pre-Sun ball in my paper SunQM-2s1). If we average all these objects over φ , then re-present each of these objects using the averaged-represented object, then all of them have θ -dimension's potential energy formula as Eq-13. Since this formula has a variable θ which covers from 0 to π , so this formula covers all objects on the r_n shell of the pre-Sun ball (after integrating θ from 0 to π).

As for the φ -dimension, since F_{cntfgl} always perpendicular to φ -dimension, so $F_{\text{cntfgl-}\varphi}$ always =0, so $V_{\text{cntfgl-}\varphi} \equiv 0$. Therefore, in $\theta\varphi$ -2D-dimension, $V_{\text{cntfgl-}\theta\varphi} = V_{\text{cntfgl-}\theta} + V_{\text{cntfgl-}\varphi} = V_{\text{cntfgl-}\theta}$. Note: in $\theta\varphi$ -2D-dimension, for integration $\iint V_{\text{cntfgl-}\theta\varphi} \sin(\theta) d\theta d\varphi$, $V_{\text{cntfgl-}\theta} + V_{\text{cntfgl-}\varphi}$ have to be separated, it cannot be fused into one item.

II-c. First order spin-perturbation energy calculation ($F_{\text{cntfgl-}\theta\varphi}$ only) for pre-Sun ball disk-lyzation (under nLL effect)

Note: in this section, we only consider $F_{\text{cntfgl-}\theta\varphi} = F_{\text{cntfgl-}\theta}$, ignore $F_{\text{cntfgl-r}}$ and ignore the Coriolis force.

II-c1. Build up the formula $E_{\text{nlm}}^{(10\varphi)} = \langle \text{nlm} | \hat{H}_{10\varphi} | \text{nlm} \rangle$

Now let us build a time-independent perturbation model for the spinning pre-Sun $\{N, n\}$ QM structure. In paper SunQM-3, we had a non-spin pre-Sun ball, and gravity force F_g (exist only in r-dimension), so $F_r = F_g$, $F_\theta = 0$, $F_\varphi = 0$, hence this forms a the zero-order perturbation. So the unperturbed Hamiltonian $H_0 = H_{0r} \neq 0$, and $H_{0\theta} = 0$, $H_{0\varphi} = 0$.

In section II-b, with SunSpnFrm's $\omega_{\text{spin}} > 0$, The total force = $\mathbf{F}_g + \mathbf{F}_{\text{cntfgl}}$, so the total $F_r = F_g + F_{\text{cntfgl-r}}$, $F_\theta = F_{\text{cntfgl-}\theta}$, $F_\varphi = 0$. For pre-Sun ball disk-lyzation, we only interesting what is happening in $\theta\varphi$ -2D-dimension, so the perturbation in r-dimension is ignored at this time. Note: later on (in section III) we will find that $F_{\text{cntfgl-r}}$ also contributes to the pre-Sun ball disk-lyzation. According to John S. Townsend's book "A Modern Approach to QM" 2nd ed. 2012. pp381, eq-11.1 and eq-11.15, the total Hamiltonian \hat{H} (unperturbed \hat{H}_0 plus spin-perturbed \hat{H}_1)

$$\hat{H} = \hat{H}_0 + \hat{H}_1 \quad \text{Eq-14}$$

and, the 1st order E_n shift is the expectation value of H_1 averaged in the unperturbed state wave function,

$$E_n^{(1)} = \langle \varphi_n^{(0)} | \hat{H}_1 | \varphi_n^{(0)} \rangle \quad \text{Eq-15}$$

Here I use a subscript in \hat{H} to indicate the order of the approximation, and use a superscript in parentheses in E and the wave function φ to indicate the order of the approximation. We have

$$\hat{H} = \hat{H}_0 + \hat{H}_1 = \hat{H}_{0r} + \hat{H}_{0\theta} + \hat{H}_{0\varphi} + \hat{H}_{1r} + \hat{H}_{1\theta} + \hat{H}_{1\varphi}, \text{ where } \hat{H}_{0\theta} = \hat{H}_{0\varphi} = \hat{H}_{1\varphi} = 0 \quad \text{Eq-16}$$

After removing those =0, we have the effective Hamiltonian

$$\hat{H}_0 + \hat{H}_1 = \hat{H}_{0r} + \hat{H}_{1r} + \hat{H}_{1\theta} \quad \text{Eq-17}$$

Therefore for the perturbed total E_n

$$E_n = E_n^{(0)} + E_n^{(1)} = \langle \text{nlm} | (\hat{H}_0 + \hat{H}_1) | \text{nlm} \rangle = \langle \text{nlm} | (\hat{H}_{0r} + \hat{H}_{1r} + \hat{H}_{1\theta}) | \text{nlm} \rangle = \langle \text{nlm} | \hat{H}_{0r} | \text{nlm} \rangle + \langle \text{nlm} | \hat{H}_{1r} | \text{nlm} \rangle + \langle \text{nlm} | \hat{H}_{1\theta} | \text{nlm} \rangle \quad \text{Eq-18}$$

where $|\text{nlm}\rangle = R_{\text{nl}} * Y_{\text{lm}}$. The (1st item) non-perturbation $E_n^{(0)} = \langle \text{nlm} | (\hat{H}_{0r}) | \text{nlm} \rangle$ has been solved for pre-Sun ball in paper SunQM-3: $E_n = -3.81E+11 * (m/n^2)$, where m is the orbit moving object's mass (in kg), and n is the total n of the orbit using Sun core $\{0,1\}$ as r_1 , and E_n in unit J. The 2nd item, the perturbed energy $E_{\text{nlm}}^{(1r)} = \langle \text{nlm} | \hat{H}_{1r} | \text{nlm} \rangle$, will be analyzed in

section III. It is the 3rd item, the perturbed energy $E_{nlm}^{(1\theta)} = \langle nlm | \hat{H}_{1\theta} | nlm \rangle$, makes the major contribution for the pre-Sun ball disk-lyzation. In the rest part of this section I will show that how I solved this 1st order perturbation problem.

From section II-b, we know that

$$\hat{H}_{1\theta} = V_{\theta} = (1/2) m * r_n^2 * \omega_{n-spin}^2 * \cos(\theta)^2 \quad \text{Eq-19}$$

Let us define

$$A_n = (1/2) m * r_n^2 * \omega_{n-spin}^2 \quad \text{Eq-20}$$

which is not a variable of θ or ϕ , so it keeps as a constant in $\langle Y_{lm} | \hat{H}_{1\theta} | Y_{lm} \rangle$ integration. Now

$$\hat{H}_{1\theta} = A_n * \cos(\theta)^2 \quad \text{Eq-21}$$

Because Y_{lm} function is a $\theta\phi$ -2D-dimension function, it is more straight forward to present everything in $\theta\phi$ -2D-dimension rather than θ -1D-dimension. So I change $E_{nlm}^{(1\theta)} = \langle nlm | \hat{H}_{1\theta} | nlm \rangle$ into $E_{nlm}^{(1\theta\phi)} = \langle nlm | \hat{H}_{1\theta\phi} | nlm \rangle$. They are equivalent because $\hat{H}_{1\phi} = 0$ so that $\hat{H}_{1\theta} = \hat{H}_{1\theta\phi}$. So now we have

$$E_{nlm}^{(1\theta\phi)} = \langle nlm | \hat{H}_{1\theta\phi} | nlm \rangle = \langle R_{nl} | Y_{lm} | A_n * \cos(\theta)^2 | R_{nl} | Y_{lm} \rangle = \langle R_{nl} | A_n | R_{nl} \rangle \langle Y_{lm} | \cos(\theta)^2 | Y_{lm} \rangle \quad \text{Eq-22}$$

My explorative calculation revealed that for one n , all $l(s)$ (from 0 to $n-1$) and all $m(s)$ (from -1 to $+1$) have the same value of $\langle R_{nl} | A_n | R_{nl} \rangle$ (see section II-c2). For pre-Sun ball disk-lyzation, we only need to know the $E_{nlm}^{(1\theta\phi)}$ within each single n shell, so we can treat $\langle R_{nl} | A_n | R_{nl} \rangle$ as the unit of $\langle Y_{lm} | \cos(\theta)^2 | Y_{lm} \rangle$. Also, after spin, the degeneracy of l and m for each n is removed, so we need to replace $E_{nlm}^{(1\theta\phi)}$ by $E_{n'l'm',nlm}^{(1\theta\phi)}$. Therefore, we have (a matrix of)

$$E_{n'l'm',nlm}^{(1\theta\phi)} = \langle R_{n'l'} | A_n | R_{nl} \rangle \langle Y_{l'm'} | \cos(\theta)^2 | Y_{lm} \rangle \quad \text{Eq-23}$$

This is the ultimate equation for the centrifugal force caused 1st order spin-perturbated $E_n^{(1)}$ in $\theta\phi$ -dimension.

II-c2. Calculation of $\langle R_{nl'} | A_n | R_{nl} \rangle$ for our SunSpnFrm under (the most possible) $\omega_{n-spin} = \omega_{1-spin} / n^3$ model

Eq-20 shows that A_n is ω_{n-spin} dependent. Table 1 shows our SunSpnFrm has $\omega_{n-spin} = \omega_{1-spin} / n^x$, with possible x from 0 to 4, and the most possible x is $=3$. So here let us calculate $\langle R_{nl'} | A_n | R_{nl} \rangle$ for our SunSpnFrm under (the most possible) $\omega_{n-spin} = \omega_{1-spin} / n^3$ model. Using $\omega_{n-spin} = \omega_{1-spin} / n^3$ and $r_n = r_1 * n^2$ to formula Eq-20, $A_n = (1/2) m * r_n^2 * \omega_{n-spin}^2 = (1/2) m * (r_1^2 * n^4) * (\omega_{1-spin}^2 / n^6) = (1/2) m * r_1^2 * \omega_{1-spin}^2 / n^2 = A_1 * (r_1 / r_n)$, where $A_1 = (1/2) m * r_1^2 * \omega_{1-spin}^2$. Let us define

$$A = A_1 = (1/2) m * r_1^2 * \omega_{1-spin}^2 \quad \text{Eq-24}$$

Then we obtain

$$A_n = A r_1 / r_n \quad \text{Eq-25}$$

Since we only interesting in $E_{n'l'm',nlm}^{(1\theta\phi)}$ within a single n shell, so δ_{nn} is enforced here. For non-diagonal elements in $E_{n'l'm',nlm}^{(1\theta\phi)}$ matrix, $l' \neq l$, $\langle R_{nl'} | A_n | R_{nl} \rangle = A r_1 \langle R_{nl'} | 1 / r_n | R_{nl} \rangle$, which is not equal to zero. For diagonal elements, $l' = l$, $\langle A_n \rangle = \langle R_{nl} | A_n | R_{nl} \rangle = A r_1 \langle R_{nl} | 1 / r_n | R_{nl} \rangle = A / n^2$, as shown below (Note: all integrations using the online calculator "WolframAlpha" (<https://www.wolframalpha.com>), or using program R).

$$\begin{aligned}
\langle \mathbf{R}_{10} | A_n | \mathbf{R}_{10} \rangle &= A r_1 \langle \mathbf{R}_{10} | 1/r_n | \mathbf{R}_{10} \rangle = A. \\
\langle \mathbf{R}_{20} | A_n | \mathbf{R}_{20} \rangle &= A r_1 \langle \mathbf{R}_{20} | 1/r_n | \mathbf{R}_{20} \rangle = (1/4) A. \\
\langle \mathbf{R}_{21} | A_n | \mathbf{R}_{21} \rangle &= A r_1 \langle \mathbf{R}_{21} | 1/r_n | \mathbf{R}_{21} \rangle = (1/4) A. \\
\langle \mathbf{R}_{30} | A_n | \mathbf{R}_{30} \rangle &= A r_1 \langle \mathbf{R}_{30} | 1/r_n | \mathbf{R}_{30} \rangle = (1/9) A. \\
\langle \mathbf{R}_{31} | A_n | \mathbf{R}_{31} \rangle &= A r_1 \langle \mathbf{R}_{31} | 1/r_n | \mathbf{R}_{31} \rangle = (1/9) A. \\
\langle \mathbf{R}_{32} | A_n | \mathbf{R}_{32} \rangle &= A r_1 \langle \mathbf{R}_{32} | 1/r_n | \mathbf{R}_{32} \rangle = (1/9) A. \\
\langle \mathbf{R}_{42} | A_n | \mathbf{R}_{42} \rangle &= A r_1 \langle \mathbf{R}_{42} | 1/r_n | \mathbf{R}_{42} \rangle = (1/16) A. \\
\langle \mathbf{R}_{43} | A_n | \mathbf{R}_{43} \rangle &= A r_1 \langle \mathbf{R}_{43} | 1/r_n | \mathbf{R}_{43} \rangle = (1/16) A. \\
\langle \mathbf{R}_{54} | A_n | \mathbf{R}_{54} \rangle &= A r_1 \langle \mathbf{R}_{54} | 1/r_n | \mathbf{R}_{54} \rangle = (1/25) A. \\
\langle \mathbf{R}_{65} | A_n | \mathbf{R}_{65} \rangle &= A r_1 \langle \mathbf{R}_{65} | 1/r_n | \mathbf{R}_{65} \rangle = (1/36) A.
\end{aligned} \tag{Eq-26}$$

So if $v_{n\text{-spin}} = v_{1\text{-spin}}/n$, like the non-perturbate $E_n^{(0)}$, the 1st-order spin-perturbed $E_n^{(1)}$ in r-dimension at n state is also $=1/n^2$ of that at $E_1^{(1)}$ for diagonal elements. So we can define

$$\langle A_n | l \rangle = \langle R_n | A_n | R_n \rangle = A / n^2 \tag{Eq-27}$$

In sections II-c3, II-c4, II-c5, and II-c6, I will calculate the $\langle Y_{lm} | \cos(\theta)^2 | Y_{lm} \rangle$ under this SunSpnFrm for $n=1, 2, 3, 5$ respectively. (Note: for x other than 3, I will make a discussion in section II-c7).

II-c3. For $n=1$, only one state $|1,0,0\rangle = |\mathbf{R}_{10}\rangle |Y_{00}\rangle$, calculate the spin-perturbed $E_{n'l'm'}^{(10\phi)} = \langle n'l'm' | \hat{H}_{10\phi} | nlm \rangle$ in $\theta\phi$ -dimension

Now let us calculate the $\langle Y_{lm} | \cos(\theta)^2 | Y_{lm} \rangle$ part for the 1st-order perturbed $E_{n'l'm'}^{(10\phi)}$ for all $n, l = 0, 1, 2, \dots, n-1$, and $m = -l, \dots, +l$. From wiki "Spherical coordinate system", the differential solid angle is

$$d\Omega = \sin(\theta) d\theta d\phi \tag{Eq-28}$$

so the integration of $\langle Y_{lm} | Y_{lm} \rangle$ in the $\theta\phi$ -2D-dimension is

$$\langle Y_{lm} | Y_{lm} \rangle = \iint Y_{l'm'}^* * Y_{lm} * \sin(\theta) d\theta d\phi, \theta=[0, \pi], \phi=[0, 2\pi] \tag{Eq-29}$$

Note: All spherical harmonic function $|Y_{lm}\rangle$ are obtained from wiki "Table of spherical harmonics". All integration was performed using an online calculator "WolframAlpha" (<https://www.wolframalpha.com/>).

The ground state $n = 1$ is not degenerate, so its spin-perturbed $E_{nlm}^{(10\phi)}$ is straight forward.

$$E_{100}^{(10\phi)} = \langle R_{10} | A_n | R_{10} \rangle \langle Y_{00} | \cos(\theta)^2 | Y_{00} \rangle$$

Or,

$$E_{100}^{(10\phi)} = \langle R_{10} | A_n | R_{10} \rangle \iint 1/\sqrt{4\pi} * \cos(\theta)^2 * 1/\sqrt{4\pi} * \sin(\theta) d\theta d\phi = A/3 \tag{Eq-30}$$

II-c4. For $n=2$, calculate the F_{spin}-perturbed $E_{n'l'm'}^{(10\phi)} = \langle Y_{l'm'} | \hat{H}_{10\phi} | Y_{lm} \rangle$ in $\theta\phi$ -dimension

For the first excited state $n = 2$, there are four degenerate states $|2,0,0\rangle, |2,1,0\rangle, |2,1,1\rangle, |2,1,-1\rangle$, we need to use the Higher-Order Degeneracy perturbation theory (see Davis J Griffiths 's book "Introduction to Quantum mechanics", 2nd ed. 2005. pp266, Chapter 6 Time-independent perturbation theory, Section 6.2.2 Higher-Order Degeneracy). According to Griffiths book's eq-6.28 and eq-6.29:

$$\begin{pmatrix} W_{aa} & W_{ab} \\ W_{ba} & W_{bb} \end{pmatrix} \begin{pmatrix} \alpha \\ \beta \end{pmatrix} = E^1 \begin{pmatrix} \alpha \\ \beta \end{pmatrix} \quad \text{Eq-31}$$

$$W_{ij} = \langle \psi_i^0 | H' | \psi_j^0 \rangle. \quad \text{Eq-32}$$

let us build a 4×4 matrix of $\langle Y_{1m'} | \hat{H}_{10\phi} | Y_{1m} \rangle$ using the four degenerate states $|2,0,0\rangle$, $|2,1,0\rangle$, $|2,1,1\rangle$, $|2,1,-1\rangle$ as a basis. So each element of the matrix is $E_{21m',21m}^{(10\phi)} = \langle 21m' | \hat{H}_{10\phi} | 21m \rangle = \langle R_{21} | A_n | R_{21} \rangle \langle Y_{1m'} | \cos(\theta)^2 | Y_{1m} \rangle$ in $\theta\phi$ -dimension. From section II-c2, we know $\langle R_{21} | A_n | R_{21} \rangle = A/4$. The calculated matrix of $\langle Y_{1m'} | \cos(\theta)^2 | Y_{1m} \rangle$ is shown in Table 2a,

Table 2a. $\langle Y_{1m'} | \cos(\theta)^2 | Y_{1m} \rangle$

$\langle Y_{1m'} \cos(\theta)^2 Y_{1m} \rangle$	$ Y_{00}\rangle$	$ Y_{10}\rangle$	$ Y_{11}\rangle$	$ Y_{1-1}\rangle$
$\langle Y_{00} $	1/3	0	0	0
$\langle Y_{10} $	0	0.6	0	0
$\langle Y_{11} $	0	0	0.2	0
$\langle Y_{1-1} $	0	0	0	0.2

and matrix of $\langle 21m' | \hat{H}_{10\phi} | 21m \rangle$ is shown in Table 2b:

Table 2b. $\langle 21m' | \hat{H}_{10\phi} | 21m \rangle = \langle R_{21} | A_n | R_{21} \rangle \langle Y_{1m'} | \cos(\theta)^2 | Y_{1m} \rangle$ with known $\langle R_{21} | A_n | R_{21} \rangle = A/4$.

$\langle 21m' \hat{H}_{10\phi} $	$ 200\rangle$	$ 210\rangle$	$ 211\rangle$	$ 21-1\rangle$
$\langle 200 $	0.083 A	0	0	0
$\langle 210 $	0	0.15 A	0	0
$\langle 211 $	0	0	0.05 A	0
$\langle 21-1 $	0	0	0	0.05 A

Note: all matrix elements with $m' \neq m$ should = 0. Because $\cos(\theta)^2$ does not contain ϕ , all $\int \exp[i(-m'+m)\phi] d\phi$ in $[0,2\pi] = 0$, but $\langle R_{n1} | R_{n1} \rangle \neq \delta_{nn} \delta_{11}$.

Comparing it to the matrix of unperturbed $E_{n1m',n1m}^{(00\phi)} = \langle n1m' | \hat{H}_{00\phi} | n1m \rangle$ in $\theta\phi$ -dimension (shown in Table 2c):

Table 2c. Unperturbed $E_{n1m',n1m}^{(00\phi)} = \langle n1m' | \hat{H}_{00\phi} | n1m \rangle$

$\langle 21m' \hat{H}_{00\phi} $	$ 200\rangle$	$ 210\rangle$	$ 211\rangle$	$ 21-1\rangle$
$\langle 200 $	0	0	0	0
$\langle 210 $	0	0	0	0
$\langle 211 $	0	0	0	0
$\langle 21-1 $	0	0	0	0

Result & discussion (for section II-c4):

1) The diagonal only matrix in Table 2b means that the spin-perturbed eigenvector (state) space is exactly the same as the unperturbed eigenvector (state) space. So we can directly compare the values of diagonal elements (which equal to the 1st order spin-perturbed energy) in the unperturbed states.

2) In $\theta\phi$ -dimension, spin perturbation increase all four states' energy from =0 to >0, with $E_{210}^{(10\phi)} (=0.15A) > E_{200}^{(10\phi)} (=0.083A) > E_{211}^{(10\phi)} (=0.05A) = E_{21-1}^{(10\phi)} (=0.05A)$. So the 4-fold degenerate of unperturbed $E_{(n=2)}^{(10\phi)} = 0$ has been removed after spin perturbation.

3) We see that in the $l = 1$ sub-shell, the higher $|m|$ (at equator) has lower perturbed E (or higher probability density). Also between sub-shells $l = 1$ and $l = 0$, the largest l number and the largest m number ($|n1m\rangle = |211\rangle$) has the lowest $E_{n1m}^{(10\phi)}$.

Later on we will see that result 3) is the major QM driving force for pre-Sun disk-lyzation.

II-c5. For state n=3, l=0, 1, 2, m= -2...+2, calculate the spin-perturbed $E_{nl'm',nlm}^{(1\theta\phi)} = \langle nl'm' | \hat{H}_{1\theta\phi} | nlm \rangle$ in $\theta\phi$ -dimension, the nLL effect

For n=3, there are total 9 states . The unperturbed E_n of these 9 states are completely degenerate in either r-dimension ($E_n = -3.81E+11 *(m/n^2)$ J for Solar QM {N,n} structure), or $E_n = 0$ in $\theta\phi$ -dimension. Same as in section II-c4, we can construct a 9×9 matrix for unperturbed $E_{nl'm',nlm}^{(0\theta\phi)} = \langle nl'm' | \hat{H}_{0\theta\phi} | nlm \rangle$ in $\theta\phi$ -dimension, where all elements (include the diagonal elements) =0 (not shown here).

From section II-c2, we know $\langle R_{3l} | A_n | R_{3l} \rangle = A/9$. So each element of the matrix $E_{3l'm',3lm}^{(1\theta\phi)} = \langle 3l'm' | \hat{H}_{1\theta\phi} | 3lm \rangle = \langle R_{3l} | A_n | R_{3l} \rangle \langle Y_{l'm'} | \cos(\theta)^2 | Y_{lm} \rangle$ in $\theta\phi$ -dimension. The result of $\langle Y_{l'm'} | \cos(\theta)^2 | Y_{lm} \rangle$ in $\theta\phi$ -dimension is shown in a 9×9 matrix in Table 3a below (using $\langle R_{3l} | A_n | R_{3l} \rangle$ as unit). The result of spin-perturbed $E_{3l'm',3lm}^{(1\theta\phi)} = \langle 3l'm' | \hat{H}_{1\theta\phi} | 3lm \rangle$ in $\theta\phi$ -dimension is shown in Table 3b.

Table 3a. The result of $\langle Y_{l'm'} | \cos(\theta)^2 | Y_{lm} \rangle$ (using $\langle R_{3l} | A_n | R_{3l} \rangle$ as unit).

$\langle 3l'm' H_{1\theta\phi} 3lm \rangle$	300>	310>	311>	31-1>	320>	321>	32-1>	322>	32-2>
<300	1/3 <A3,0>	0	0	0	0.298 <30 An 32>				
<310	0	0.6 <A3,1>	0	0					
<311	0	0	0.2 <A3,1>	0					
<31-1	0	0	0	0.2 <A3,1>					
<320	0.298 <32 An 30>	0	0	0	11/21 <A3,2>	0	0	0	0
<321	0	0	0	0	0	3/7 <A3,2>			
<32-1	0	0	0	0	0	0	3/7 <A3,2>		
<322	0	0	0	0	0	0	0	1/7 <A3,2>	
<32-2	0	0	0	0	0	0	0	0	1/7 <A3,2>

Table 3b. The result of spin-perturbed $E_{3l'm',3lm}^{(1\theta\phi)} = \langle 3l'm' | \hat{H}_{1\theta\phi} | 3lm \rangle$ in $\theta\phi$ -dimension

$\langle 3l'm' H_{1\theta\phi} 3lm \rangle$	300>	310>	311>	31-1>	320>	321>	32-1>	322>	32-2>
<300	0.037 A	0	0	0	0.010 A				
<310	0	0.067 A	0	0					
<311	0	0	0.022 A	0					
<31-1	0	0	0	0.022 A					
<320	0.010 A				0.058 A				
<321						0.048 A			
<32-1							0.048 A		
<322								0.016 A	
<32-2									0.016 A

Note: all empty cells in Table 3 have value =0.

Note: Calculated $\langle R_{32} | A_n | R_{30} \rangle = A r_1 \langle R_{32} | 1/r_n | R_{30} \rangle = 0.035 A$.

There are two non-diagonal elements ≠0. Extract out them to form a sub-matrix in Table 3c:

Table 3c. A sun-matrix extracted out from Table 3b where non-diagonal elements ≠0. Unit=A.

$\langle 3l'm' H_{1\theta\phi} 3lm \rangle$	300>	320>
<300	0.037	0.01
<320	0.01	0.058

Solve the eigenvalue problem for this sub-matrix (by using Wolfram's online calculator "Eigenvalue and Eigenvector (2×2)", or by using R program), and put them into a new sub-matrix in Table 3d:

Table 3d. The eigenstate matrix of Table 3c.

$\langle 3l'm' H_{1\theta\phi} 3lm \rangle$	$-0.93 300 \rangle + 0.37 320 \rangle$	$0.37 300 \rangle + 0.93 320 \rangle$
$-0.93 300 \rangle + 0.37 320 \rangle$	0.033	0
$0.37 300 \rangle + 0.93 320 \rangle$	0	0.062

Then put these diagonalized elements back to Table 3b, we obtain Table 3e.

Table 3e. The eigenvector solution of Table 3b.

$\langle 3l'm' H_{1\theta\phi} 3lm \rangle$	$-0.93 300 \rangle + 0.37 320 \rangle$	$ 310 \rangle$	$ 311 \rangle$	$ 31-1 \rangle$	$0.37 300 \rangle + 0.93 320 \rangle$	$ 321 \rangle$	$ 32-1 \rangle$	$ 322 \rangle$	$ 32-2 \rangle$
$-0.93 300 \rangle + 0.37 320 \rangle$	0.033 A	0	0	0					
$ 310 \rangle$	0	0.067 A	0	0					
$ 311 \rangle$	0	0	0.022 A	0					
$ 31-1 \rangle$	0	0	0	0.022 A					
$0.37 300 \rangle + 0.93 320 \rangle$					0.062 A				
$ 321 \rangle$						0.048 A			
$ 32-1 \rangle$							0.048 A		
$ 322 \rangle$								0.016 A	
$ 32-2 \rangle$									0.016 A

Result & discussion (for section II-c5):

1) In $\theta\phi$ -dimension, spin perturbation increase all 9 states' energy from =0 to >0, so the 9-fold degenerate of unperturbed $E_{(n=3)}=0$ has been removed.

2) In Table 3e we see that within each l sub-shell, the higher the $|m|$ value (meaning the closer to equator), the lower the perturbed E (meaning the higher probability density). Also between l sub-shells, the largest l number and the largest $|m|$ number ($|nlm\rangle = |322\rangle$) has the lowest $E_{nlm}^{(1\theta\phi)}$. So for each n , it not only makes the $m = \pm l$ the lowest $E_{nl'm',nlm}^{(1\theta\phi)}$ among all possible $m(s)$ (as I originally expected), at the same time, it also make the $l = n-1$ the lowest $E_{nl'm',nlm}^{(1\theta\phi)}$ among all possible $l(s)$ (I thought I need to do more math to get that)!

Let us define the L as the maximum value of l (among all possible values of 0, 1, ... n-1) for a quantum orbit n . Also let us define the L as the maximum value of $|m|$ (among all possible values of $-l, \dots, +l$) for a quantum orbit $l = L$. Table 3e tells us that for each n shell (containing l sub-shells and m layers), only nLL orbits have the lowest $E_{nl'm',nlm}^{(1\theta\phi)}$. I name it as (spin caused) "nLL effect". Example of nLL are: $nlm = 211, 322, 433, 544, \dots$

From John S. Townsend's book "A Modern Approach to QM" 2nd ed. 2012. pp356, eq-10.45 through eq-10.50, we know that not every r_{nlm} satisfies $r_n = r_1 * n^2$, only nLL orbits satisfy this relationship. (Note, nLL orbit with $m = -L$ will be explained later). The 3D plot of $|Y_{lm}|^2$ (from any QM text book) shows that the $|Y_{LL}|^2$ forms highest probability density at (or near) equator of the l sub-shell.

3) Although in Table 3e matrix, both $|nlm\rangle = |3,2,+2\rangle$ and $|3,2,-2\rangle$ have the same lowest energy of perturbation, we can differentiate these two state energy in the following way: In SunSpnFrm, both $|n,L,m=+L\rangle$ and $|n,L,m=-L\rangle$ states can be simplified as doing circular movement only in x-y plane. They have the same orbit v value, but in opposite direction. Let us define that $|n,L,m=+L\rangle$ state's v_{orbit} has the same direction as that of SunSPnFrm's ω_{n-spin} , so its orbit v relative to the non-spin frame is $|v_{n-orbit}| + |r_n \omega_{n-spin}|$. Then, $|n,L,m=-L\rangle$ state will have its orbit $v = |v_{n-orbit}| - |r_n \omega_{n-spin}|$ in the non-pin frame. The general circular orbit energy $E_n = -(1/2) m v_n^2$ means that the higher the orbit v , the lower the orbital E . So the state E between

$|n, L, m=+L\rangle$ and $|n, L, m=-L\rangle$ is differentiated in the spin frame. Therefore only nLL state (not both nLL and nL-L states) has the lowest state E among $m = -L, \dots, +L$.

The molecular basis (or the particle physics view) of this phenomenon has been explained in paper SunQM-3: During collapsing of the pre-Sun ball, only < 1% of objects (at the high end of Boltzmann velocity distribution) in each n shell will have high enough v, and close enough to nLL orbit, to survive from the collapse, and transform their RF heat (micro random) movement v into the (non-random) macro movement (as orbit v), and re-gain the sustaining force (now it is $F = m a = m v_n^2 / r_n$) to stay in the original n shell!

4) **So now let us construct a simple pre-Sun QM model, with each n shell allow only one object to stay in. the best chance we will find these objects are in orbit $nlm = 211, 322, 433, 544$, etc.** These nLL orbits locate at (or near) the equator of the spinning pre-Sun ball, and satisfy $r_n = r_1 * n^2$ relationship. This is almost same as the Bohr model, except now it is for a spinning pre-Sun QM $\{N, n\}$ model! **So from Schrodinger equation and solution, we can deduce a Bohr-like model for the Solar QM $\{N, n\}$ structure. And this is the basis of my work in paper SunQM-1**, where I only used $r_n = r_1 * n^2$ relationship to explore the Solar system QM.

Of cause, one of the most important differences between Schrodinger equation solution and Bohr model is that as n decrease, the uncertainty (or RF) of the orbit in $\theta\phi$ -2D dimension greatly increases. It has been discussed in my paper SunQM-2, and SunQM-2s1.

One important result come out of this analysis (actually partly come out from paper SunQM-3s2) is that in the spinning pre-Sun, if the mass occupancy is <1% for orbit n, then all mass in space between $\{N, n\}$ and $\{N, n+1\}$ at different m layers falls into $m = L$ layer at equator, meanwhile the same mass also falls into the most inner ($l = L$) sub-shell. This means that the orbit n collected all mass in n shell space (between r_n to r_{n+1}). In other word, the mass of Earth at $\{1, 5\}$ orbit is the result of collection all mass in the spherical shell space between $\{1, 5\}$ Earth and $\{1, 6\}$ Mars. So in my previous paper SunQM-1s1 Table 3b, when using the Solar system's mass radial distribution formula $D = 4.37E+28 / r^{(3.279)}$ to calculate the total mass in each n shell, I need to use r_n to r_{n+1} for the spherical shell volume calculation.

5) Kinetically nLL effect has two steps: first from a spherical shell $|n/m\rangle$ to a disk $|n/L\rangle$, and then (or at the same time) from a disk $|n/L\rangle$ to a set of separated rings $|nLL\rangle$. Although both process are driven by the same spin-perturbated QM force, the forming of disk $|n/L\rangle$ is faster than forming a set of separated rings $|nLL\rangle$ in kinetics.

II-c6. For state $n=5, l=0, \dots, 4, m = -l \dots +l$, calculate the spin-perturbed $E_{nl'm', nlm}^{(10\phi)} = \langle nl'm' | \hat{H}_{10\phi} | nlm \rangle$ in $\theta\phi$ -dimension

My purpose in this section is to show people that for $n = 5$, it still obey the rule that only the nLL state has the lowest (1st-order) spin-perturbed energy. For $n = 5$, there are total 25 states. The result of $\langle Y_{lm} | \cos(\theta)^2 | Y_{lm} \rangle$ in $\theta\phi$ -dimension is shown in a 25×25 matrix in Table 4 below (using $\langle R_{5l} | A_n | R_{5l} \rangle$ as unit).

Table 4. The result of spin-perturbed $E_{nl'm', nlm}^{(10\phi)} = \langle nl'm' | \hat{H}_{10\phi} | nlm \rangle$ for $n=5$ in a 25×25 matrix.

$\langle n'l'm' H_{\text{int}} n'l m \rangle$	500>	510>	511>	51-1>	520>	521>	52-1>	522>	52-2>	530>	531>	53-1>	532>	53-2>	533>	53-3>	540>	541>	54-1>	542>	54-2>	543>	54-3>	544>	54-4>
<500	1/3 <A5,0>	0	0	0	0.298 <50 An 52>					0.262 <51 An 53>															
<510	0	0.6 <A5,1>	0	0	0					0.214 <51 An 53>									0						
<511	0	0	0.2 <A5,1>	0		0				0.214 <51 An 53>									0						
<51-1	0	0	0	0.2 <A5,1>						0.214 <51 An 53>									0						
<520	0.298 <52 An 50>	0			11/21 <A5,2>	0	0	0	0								0.256 <52 An 54>								
<521			0		3/7 <A5,2>						0						0.233 <52 An 54>								
<52-1					3/7 <A5,2>						0						0.233 <52 An 54>								
<522						1/7 <A5,2>														0.165 <52 An 54>					
<52-2						1/7 <A5,2>														0.165 <52 An 54>					
<530	0.262 <53 An 51>				0					23/45 <A5,3>	0	0	0	0	0	0									
<531		0.214 <53 An 51>				0				7/15 <A5,3>															
<53-1			0.214 <53 An 51>							7/15 <A5,3>															
<532											1/3 <A5,3>														
<53-2											1/3 <A5,3>														
<533												1/9 <A5,3>													
<53-3												1/9 <A5,3>													
<540	0	0			0.256 <54 An 52>												39/77 <A5,4>								
<541			0		0.233 <54 An 52>						0						37/77 <A5,4>								
<54-1					0.233 <54 An 52>						0						37/77 <A5,4>								
<542						0.165 <54 An 52>							0							31/77 <A5,4>					
<54-2						0.165 <54 An 52>							0							31/77 <A5,4>					
<543																						21/77 <A5,4>			
<54-3																						21/77 <A5,4>			
<544																							7/77 <A5,4>		
<54-4																							7/77 <A5,4>		

Note: in Table 4, all empty elements have value =0. There are some non-diagonal elements $\neq 0$ and they all have $m = m'$ for their $\langle Y_{1m} | \cos(\theta)^2 | Y_{1m} \rangle$.

Note: as shown in section II-c2, $\langle A5,0 \rangle = \langle A5,1 \rangle = \langle A5,2 \rangle = \langle A5,3 \rangle = \langle A5,4 \rangle = A/25$.

Immediately we notice that there are many non-diagonal elements not equal to zero. $\langle R_{nl} | R_{nl} \rangle$ is not orthogonal, so $\langle R_{nl} | A_n | R_{nl} \rangle$ will not add any more zero element in the matrix of Table 4. It is not easy to solve the eigenvalue problem for this 25×25 matrix. Even it is diagonalized in its eigen-vector space, it is still not very helpful for explaining the result.

Here I use two ways to show that this 25×25 matrix still obey the rule that $E_{nLL}^{(10\phi)}$ is the lowest.

1) If we use following eight states (in Table 4), $|532\rangle, |53-2\rangle, |533\rangle, |53-3\rangle, |543\rangle, |54-3\rangle, |544\rangle, |54-4\rangle$ to form a 8×8 sub-matrix (not shown), this 8×8 matrix is a natural diagonal matrix, means we can compare their $E_{nlm}^{(10\phi)}$ directly under the unperturbed states. This 8×8 sub-matrix still shows that within each l sub-shell, the higher the $|m|$ value, the lower the perturbed E . Also between l sub-shells, the largest l number and the largest $|m|$ number ($|nlm\rangle = |544\rangle$) has the lowest $E_{nlm}^{(10\phi)}$. So at least for those high m and high l elements in the 25×25 matrix, they follow the rule that nLL has the lowest $E_{nlm}^{(10\phi)}$.

2) To prove nLL has the lowest $E_{nlm}^{(10\phi)}$, I only need to compare the sequential order of each state's $E_{nl'm',nlm}^{(10\phi)}$, I don't need to know the exact value of $E_{nl'm',nlm}^{(10\phi)}$. In Table 3c, the non-diagonal elements ($=0.010 A1$) are only $1/3 \sim 1/6$ of diagonal elements (0.01/0.037, or 0.01/0.058). As a physicist, I can see that this matrix can be treated as the diagonal only matrix plus some (limited) deviation contributed by the small non-diagonal elements. The deviation will not change the original sequential order which is set by the main contributor (the diagonal elements). This means that if I ignore the non-diagonal elements, the diagonal only matrix will still give the right order sequence! This analysis is valid for matrix from Table 3a through Table 3e, and it should be also valid for matrix in Table 4. So comparing the diagonal elements in Table 4, we see clearly that nLL = $|544\rangle$ has the lowest $E_{nlm}^{(10\phi)}$.

There are some other properties that worthwhile to discuss here.

1) In section II-c3, we see $E_{100}^{(10\phi)} = A/3$. Then carefully analyzing of Table 4 (also Table 3, and Table 2) shows that all l sub-shells (in a single $n = 5$ shell) have the same averaged $E_{nlm}^{(10\phi)} = A/3$ (as shown in column 4 of Table 5a). So before spin, for a pre-Sun ball, not only all l sub-shells of each n shell have the same $E_{nl}^{(10\phi)}$ value, but also for all m layers in each l sub-shell have the same $E_{nl}^{(10\phi)}$ value (or we say all m layers are degenerated). After spin, each l sub-shell still has the same $E_{nl}^{(10\phi)}$ value (see Eq-26), but now m layers are differentiated, each m layer has its own $E_{nlm}^{(10\phi)}$ value (with the E_{nLL} has the lowest value), although the total averaged $E_{nlm}^{(10\phi)}$ value still equals to the pre-spin $E_{nl}^{(10\phi)}$ value.

This really helped me to understand the meaning of remove degenerate in QM: it divides the space (like θ) into many (virtual) sub-spaces (like m), and then re-average the physics value (like E) in each sub-space, while keep the total averaged value unchanged. Now let me re-phrase it. In classical physics, $V_{\theta\text{-spin}} (= (1/2) m * r^2 * \omega_{\text{spin}}^2 * \cos(\theta)^2)$ continuously decrease as θ increasing, minimum at $\theta=\pi/2$. In QM, e.g., $l=4, m = -4 \dots +4$, θ has been quantized into 9 quanta, then $\hat{H}_{10} = (1/2) m * r_n^2 * \omega_{n\text{-spin}}^2 * \cos(\theta)^2$ is averaged in each quantum of θ by $\langle lm | \hat{H}_{10} | lm \rangle$! So that in QM's E_{lm} , there is no θ , it is replaced by m .

Table 5a. Extraction of the characterized results from the diagonal elements in Table 4 and Table 5b.

	$E_{nlm}^{(10\phi)} = \langle nlm \hat{H}_{10\phi} nlm \rangle$		avg $E_{nlm}^{(10\phi)}$ for each l sub-shell	ratio $E_{n(L-1)}^{(10\phi)} / E_{nLL}^{(10\phi)}$
Unit	A/n^2, in fraction	A/n^2, in real value	A/n^2	
n,l,m				
1,0,0	1/3	0.333	1/3	
2,0,0	1/3	0.333	1/3	
2,1,0	3/5	0.600		
2,1,1	1/5	0.200	1/3	3
2,1,-1	1/5	0.200		
.....
5,0,0	1/3	0.333	1/3	
5,1,0	3/5	0.600		
5,1,1	1/5	0.200	1/3	
5,1,-1	1/5	0.200		
5,2,0	11/21	0.524		
5,2,1	3/7	0.429		
5,2,-1	3/7	0.429		
5,2,2	1/7	0.143	1/3	3
5,2,-2	1/7	0.143		
5,3,0	23/45	0.511		
5,3,1	7/15	0.467		
5,3,-1	7/15	0.467		
5,3,2	1/3	0.333		
5,3,-2	1/3	0.333		
5,3,3	1/9	0.111	1/3	3
5,3,-3	1/9	0.111		
5,4,0	39/77	0.506		
5,4,1	37/77	0.481		
5,4,-1	37/77	0.481		
5,4,2	31/77	0.403		
5,4,-2	31/77	0.403		
5,4,3	3/11	0.273		
5,4,-3	3/11	0.273		
5,4,4	1/11	0.091	1/3	3
5,4,-4	1/11	0.091		
.....
11,10,0	219/437	0.501		
11,10,1	217/437	0.497		
.....
11,10,9	3/23	0.130		
11,10,10	1/23	0.043		3

Wiki "Table of spherical harmonics" listed spherical harmonic function $|Y_{lm}\rangle$ up to $l=10$, so $n=11$ is the highest n that I can calculate for $E_{nl'm,nlm}^{(10\phi)}$. Table 5b shows the result of spin-perturbed diagonal elements $E_{nlm}^{(10\phi)} = \langle 11lm | \hat{H}_{10\phi} | 11lm \rangle$ for $n=11, l=10$, two lowest m ($m=0, 1$) and two highest m ($m=9,10$) values in a truncated matrix.

Table 5b. The result of spin-perturbed $E_{nlm}^{(10\phi)} = \langle 11lm | \hat{H}_{10\phi} | 11lm \rangle$ for $n=11$ in a truncated matrix.

$\langle 11m H_{1\theta\phi} $					
$11m \rangle$	$ 11,10,0\rangle$	$ 11,10,1\rangle$...	$ 11,10,9\rangle$	$ 11,10,10\rangle$
$\langle 11,10,0 $	$219/437 \langle A11,10 \rangle$				
$\langle 11,10,1 $		$217/437 \langle A11,10 \rangle$			
...			...		
$\langle 11,10,9 $				$3/23 \langle A11,10 \rangle$	
$\langle 11,10,10 $					$1/23 \langle A11,10 \rangle$

2) Table 4 also shows one important character: the ratio of $E_{nL(L-1)}^{(10\phi)} / E_{nLL}^{(10\phi)}$ always =3 (calculated shown in column 5 of Table 5a), no matter what n it is. Also the ratio of $E_{nl(m-1)}^{(10\phi)} / E_{nlm}^{(10\phi)}$ is highest at equator, lowest at pole for all n and l (data not shown). This ratio reflects the disk-lyzation driving force of pre-Sun ball in $\theta\phi$ -dimension: the higher the ratio value, the stronger the disk-lyzation driving force. So in $\theta\phi$ -dimension, spin causes the strongest disk-lyzation driving force of pre-Sun ball at near equator for each m layer. Since this ratio is independent of n (the n-dependent $\langle An,l \rangle$ is cancelled out), so this strong disk-lyzation driving force near equator goes all the way to high n. This is the reason of why centrifugal force is the main driving force (in comparing to the Coriolis force, data not shown) for pre-Sun disk-lyzation.

II-c7. $E_{nl'm',nlm}^{(10\phi)}$ for pre-Sun ball disk-lyzation: for a SunSpnFrm model with $\omega_{n\text{-spin}} = \omega_{1\text{-spin}} / n^x$, where $x=2$ to 4, other than $x=3$

The analysis in sections from II-c2 through II-c6 are under a SunSpnFrm model $\omega_{n\text{-spin}} = \omega_{1\text{-spin}} / n^x$ where $x=3$. Although $x=3$ is the most possible model, but I am not absolutely sure. However I know that our SunSpnFrm must have x between 2 and 4. So it is necessary to analyze the SunSpnFrm model under $x=2$, and $x=4$, to see if they still follow the rule that $E_{nLL}^{(10\phi)}$ is the lowest.

1) For $x=2$, using $\omega_{n\text{-spin}} = \omega_{1\text{-spin}} / n^2$ and $r_n = r_1 * n^2$ to formula

$$A_n = (1/2) m * r_n^2 * \omega_{n\text{-spin}}^2 = (1/2) m * (r_1 * n^2)^2 * (\omega_{1\text{-spin}} / n^2)^2 = (1/2) m * r_1^2 * \omega_{1\text{-spin}}^2 = A_1 = A. \quad \text{Eq-33}$$

So $A_n = A$ and it is no longer a r_n variable function. For this reason, all analysis for $x=3$ in sections from II-c2 through II-c6 are exactly the same for $x=2$. Therefore, a SunSpnFrm with $x=2$ is also holding the rule that nLL has the lowest $E_{nlm}^{(10\phi)}$.

2) For $x=4$, using $\omega_{n\text{-spin}} = \omega_{1\text{-spin}} / n^4$ and $r_n = r_1 * n^2$ to formula

$$A_n = (1/2) m * r_n^2 * \omega_{n\text{-spin}}^2 = (1/2) m * (r_1 * n^2)^2 * (\omega_{1\text{-spin}} / n^4)^2 = [(1/2) m * r_1^2 * \omega_{1\text{-spin}}^2] / n^4 = A_1 / n^4 = A (r_1/r_n)^2, \text{ so}$$

$$A_n = A (r_1/r_n)^2 \quad \text{Eq-34}$$

We still only interesting in $E_{nlm}^{(10\phi)}$ within a single n shell, so $\delta_{n'n}$ is enforced here. For non-diagonal elements, $l' \neq l$, $\langle R_{nl} | A_n | R_{nl} \rangle = A_1 * r_1^2 \langle R_{nl} | 1/r_n^2 | R_{nl} \rangle$, which is not equal to zero. For diagonal elements, $l' = l$,

$$\langle A_{n,l} \rangle = \langle R_{nl} | A_n | R_{nl} \rangle = A_1 * r_1^2 \langle R_{nl} | 1/r_n^2 | R_{nl} \rangle \quad \text{Eq-35}$$

The result is shown below:

$$\begin{aligned} \langle R_{10} | A_n | R_{10} \rangle &= A r_1^2 \langle R_{10} | 1/r_n^2 | R_{10} \rangle = A. \\ \langle R_{20} | A_n | R_{20} \rangle &= A r_1^2 \langle R_{20} | 1/r_n^2 | R_{20} \rangle = (1/4) A. \\ \langle R_{21} | A_n | R_{21} \rangle &= A r_1^2 \langle R_{21} | 1/r_n^2 | R_{21} \rangle = (1/12) A. \\ \langle R_{30} | A_n | R_{30} \rangle &= A r_1^2 \langle R_{30} | 1/r_n^2 | R_{30} \rangle = (2/27) A. \\ \langle R_{31} | A_n | R_{31} \rangle &= A r_1^2 \langle R_{31} | 1/r_n^2 | R_{31} \rangle = (2/81) A. \\ \langle R_{32} | A_n | R_{32} \rangle &= A r_1^2 \langle R_{32} | 1/r_n^2 | R_{32} \rangle = (2/135) A. \\ \langle R_{42} | A_n | R_{42} \rangle &= A r_1^2 \langle R_{42} | 1/r_n^2 | R_{42} \rangle = (1/160) A. \\ \langle R_{43} | A_n | R_{43} \rangle &= A r_1^2 \langle R_{43} | 1/r_n^2 | R_{43} \rangle = (1/224) A. \\ \langle R_{54} | A_n | R_{54} \rangle &= A r_1^2 \langle R_{54} | 1/r_n^2 | R_{54} \rangle = (2/1125) A. \end{aligned}$$

$$\langle R_{65}|A_n|R_{65}\rangle = A r_1^2 \langle R_{65}|1/r_n^2|R_{65}\rangle = (1/1188) A. \quad \text{Eq-36}$$

The rest analysis is the same as that in sections from II-c2 through II-c6. Therefore, a SunSpnFrm with $x=4$ is also holding the rule that nLL has the lowest $E_{nlm}^{(10\phi)}$.

Thus, we have proved that our SunSpnFrm, as long as its x between 2 and 4, it holes the rule that nLL has the lowest $E_{nlm}^{(10\phi)}$.

III. $F_{\text{cntfgl-r}}$'s contribution to the pre-Sun ball's flattening and disk-lyzation

In this section, let us discuss the $F_{\text{cntfgl-r}}$'s contribution to the pre-Sun ball's flattening and disk-lyzation.

III-a. Deduce \hat{H}_{1r} from $F_{\text{cntfgl-r}}$

From Eq-6 and Figure 2,

$$F_{\text{cntfgl-r}} = F_{\text{cntfgl}} \cos(\theta) = F_{\text{cntfgl}} \sin(\theta) = -m \cdot d \cdot \omega_{\text{spin}}^2 \sin(\theta) = -m \cdot r \cdot \omega_{\text{spin}}^2 \sin(\theta) \sin(\theta) \quad \text{Eq-37}$$

It points away from the origin. This $F_{\text{cntfgl-r}}$ caused $V_{\text{cntfugl-r}}$ is:

$$V_{\text{cntfugl-r}} = \int F_{\text{cntfgl-r}} dr = \int (-m \cdot r \cdot \omega_{\text{spin}}^2 \sin(\theta)^2) dr = -m \sin(\theta)^2 \int (r_n \cdot \omega_{\text{n-spin}}^2) dr = -m \sin(\theta)^2 \int (r_n \cdot \omega_{1\text{-spin}}^2 \cdot (r_1/r_n)^x) dr = -m \sin(\theta)^2 \cdot \omega_{1\text{-spin}}^2 \int (r_n \cdot (r_1/r_n)^x) dr \quad \text{Eq-38}$$

From $\omega_{\text{n-spin}} = \omega_{1\text{-spin}} / n^x$, we can obtain

$$\omega_{\text{n-spin}}^2 = \omega_{1\text{-spin}}^2 \cdot (r_1/r_n)^x \quad \text{Eq-39}$$

In this section, I only analyze the 1st order spin-perturbation under SunSpnFrm of $x=3$. For $x=3$, apparently

$$V_{\text{cntfugl-r}} = \int F_{\text{cntfgl-r}} dr [0, \infty] = -m \sin(\theta)^2 \cdot \omega_{1\text{-spin}}^2 \int (r_n \cdot (r_1/r_n)^3) dr = +m \sin(\theta)^2 \cdot \omega_{1\text{-spin}}^2 \cdot r_1^3 / r_n$$

The sign change is due to $\int (1/r^2) dr = -1/r + \text{cnst}$.

Now let us check the sign of $V_{\text{cntfugl-r}}$: just like that moving to the direction of F_g will get lower V_g , here moving to the direction of $F_{\text{cntfgl-r}}$ (always point away from spin axis) will get higher $V_{\text{cntfugl-r}}$, so $V_{\text{cntfugl-r}}$ has the wrong sign! The reason is that instead of integrate from $r=0$ to infinity, it should from infinity to 0, so it gains a negative sign for $V_{\text{cntfugl-r}}$. So the right formula is:

$$V_{\text{cntfugl-r}} = \int F_{\text{cntfgl-r}} dr [\infty, 0] = -m \sin(\theta)^2 \cdot \omega_{1\text{-spin}}^2 \cdot r_1^3 / r_n \quad \text{Eq-40}$$

Define:

$$B_n = m \cdot \omega_{1\text{-spin}}^2 \cdot r_1^3 / r_n = B \cdot r_1 / r_n \quad \text{Eq-41}$$

Define:

$$B = B_1 = m \cdot \omega_{1\text{-spin}}^2 \cdot r_1^2 \quad \text{Eq-42}$$

$$\hat{H}_{1r} = V_{\text{cntfugl-r}} = -m \sin(\theta)^2 \cdot \omega_{1\text{-spin}}^2 \cdot r_1^3 / r_n = -\sin(\theta)^2 \cdot B_n \quad \text{Eq-43}$$

So,

$$E_{nl'm',nlm(1r)} = \langle nl'm' | \hat{H}_{1r} | nlm \rangle = - \langle nl'm' | \sin(\theta)^2 \cdot B_n | nlm \rangle = - \langle R_{nl'} | B_n | R_{nl} \rangle \langle Y_{1m'} | \sin(\theta)^2 | Y_{1m} \rangle \quad \text{Eq-44}$$

Note: for $\langle R_{nl}|B_n|R_{nl}\rangle$, the integration still from 0 to infinity as usual, not the opposite. Now we have

$$\langle nl|B_n|nl\rangle = B r_1 * \langle R_{nl}|1/r_n|R_{nl}\rangle \quad \text{Eq-45}$$

For diagonal elements, it has the similar result as Eq-26 (although A is replaced with B here):

$$\begin{aligned} \langle R_{10}|B_n|R_{10}\rangle &= B r_1 \langle R_{10}|1/r_n|R_{10}\rangle = B. \\ \langle R_{20}|B_n|R_{20}\rangle &= B r_1 \langle R_{20}|1/r_n|R_{20}\rangle = (1/4) B. \\ \langle R_{21}|B_n|R_{21}\rangle &= B r_1 \langle R_{21}|1/r_n|R_{21}\rangle = (1/4) B. \\ \langle R_{30}|B_n|R_{30}\rangle &= B r_1 \langle R_{30}|1/r_n|R_{30}\rangle = (1/9) B. \\ \langle R_{31}|B_n|R_{31}\rangle &= B r_1 \langle R_{31}|1/r_n|R_{31}\rangle = (1/9) B. \\ \langle R_{32}|B_n|R_{32}\rangle &= B r_1 \langle R_{32}|1/r_n|R_{32}\rangle = (1/9) B. \\ \langle R_{42}|B_n|R_{42}\rangle &= B r_1 \langle R_{42}|1/r_n|R_{42}\rangle = (1/16) B. \\ \langle R_{43}|B_n|R_{43}\rangle &= B r_1 \langle R_{43}|1/r_n|R_{43}\rangle = (1/16) B. \\ \langle R_{54}|B_n|R_{54}\rangle &= B r_1 \langle R_{54}|1/r_n|R_{54}\rangle = (1/25) B. \\ \langle R_{65}|B_n|R_{65}\rangle &= B r_1 \langle R_{65}|1/r_n|R_{65}\rangle = (1/36) B. \end{aligned} \quad \text{Eq-46}$$

So for the diagonal elements,

$$E_{nlm,nlm}^{(1r)} = \langle nlm|\hat{H}_{1r}|nlm\rangle = -\langle Y_{lm}|\sin(\theta)^2|Y_{lm}\rangle B/n^2 \quad \text{Eq-47}$$

For the non-diagonal elements,

$$E_{nl'm',nlm}^{(1r)} = \langle nl'm'|\hat{H}_{1r}|nlm\rangle = -\langle Y_{l'm'}|\sin(\theta)^2|Y_{lm}\rangle \langle R_{nl'}|1/r_n|R_{nl}\rangle \quad \text{Eq-48}$$

III-b. Build $E_{nl'm',nlm}^{(1r)}$ matrix for $n=3, l=0, 1, 2$ and $m = -2, \dots, +2$

Now let us study the pre-Sun ball's $n=3$ shell. A spin-perturbed $E_{nl'm',nlm}^{(1r)} = \langle nl'm'|\hat{H}_{1r}|nlm\rangle$ for $n=3$ in a 9×9 matrix has been constructed in Table 6a.

Table 6a. The result of spin-perturbed $E_{nl'm',nlm}^{(1r)} = \langle nl'm'|\hat{H}_{1r}|nlm\rangle$ for $n=3$ in a 9×9 matrix.

$\langle nl'm' \hat{H}_{1r} nlm\rangle$	300>	310>	311>	31-1>	320>	321>	32-1>	322>	32-2>
<300	-2/3 B/9	0	0	0	0.298 <30 Bn 32>				
<310	0	-0.4 B/9	0	0					
<311	0	0	-0.8 B/9	0					
<31-1	0	0	0	-0.8 B/9					
<320	0.298 <32 Bn 30>				-10/21 B/9	0	0	0	0
<321						-4/7 B/9			
<32-1							-4/7 B/9		
<322								-6/7 B/9	
<32-2									-6/7 B/9

Note: Calculated $\langle R_{32}|B_n|R_{30}\rangle = B r_1 \langle R_{32}|1/r_n|R_{30}\rangle = 0.035 B$.

Note: $\langle R_{31}|B_n|R_{31}\rangle = B/9$.

It is interesting to see that due to $\langle Y_{l'm'}|Y_{lm}\rangle = \delta_{l'l}\delta_{m'm}$, and due to $\sin(\theta)^2 + \cos(\theta)^2 = 1$, for diagonal elements, $\langle Y_{lm}|\sin(\theta)^2|Y_{lm}\rangle = 1 - \langle Y_{lm}|\cos(\theta)^2|Y_{lm}\rangle$, for non-diagonal elements, $\langle Y_{l'm'}|\sin(\theta)^2|Y_{lm}\rangle = -\langle Y_{l'm'}|\cos(\theta)^2|Y_{lm}\rangle$. There are two non-diagonal elements $\neq 0$. Extract out them to form a sub-matrix in Table 6b:

Table 6b. Extract out non-zero elements from Table 6a to form a sub-matrix (in unit B).

$\langle 3l'm' H_{1r} 3lm\rangle$	$ 300\rangle$	$ 320\rangle$
$\langle 300 $	-0.074	0.010
$\langle 320 $	0.010	-0.053

Solve the eigenvalue problem for this sub-matrix, and put them into a new sub-matrix in Table 6c.

Table 6c. Represent Table 6b in its eigenvector space.

$\langle 3l'm' H_{1r} 3lm\rangle$	$-0.93 300\rangle + 0.37 320\rangle$	$-0.37 300\rangle - 0.93 320\rangle$
$-0.93 300\rangle + 0.37 320\rangle$	-0.078	0
$-0.37 300\rangle - 0.93 320\rangle$	0	-0.049

Then put these diagonalized elements back to Table 6a, we obtain Table 6d.

Table 6d. Represent Table 6a in its eigenvector space (unit = B).

$\langle nl'm' H_{1r} nlm\rangle$	$-0.93 300\rangle + 0.37 320\rangle$	$ 310\rangle$	$ 311\rangle$	$ 31-1\rangle$	$-0.37 300\rangle - 0.93 320\rangle$	$ 321\rangle$	$ 32-1\rangle$	$ 322\rangle$	$ 32-2\rangle$
$-0.93 300\rangle + 0.37 320\rangle$	-0.078								
$\langle 310 $		-0.044							
$\langle 311 $			-0.089						
$\langle 31-1 $				-0.089					
$-0.37 300\rangle - 0.93 320\rangle$					-0.049				
$\langle 321 $						-0.063			
$\langle 32-1 $							-0.063		
$\langle 322 $								-0.095	
$\langle 32-2 $									-0.095

Result & discussion (for Table 6d):

- 1) From Table 6d, we see that within each l sub-shell, the higher the $|m|$, the lower the $E_{nlm}^{(1r)}$. Between l sub-shells, the higher the l , also the lower the $E_{nlm}^{(1r)}$. So same as that of $\hat{H}_{1\theta\phi}$, \hat{H}_{1r} part of spin-perturbation also makes nLL the most high probability state due to its lowest $E_{nlm}^{(1r)}$.
- 2) In the discussion of Table 5a, I mentioned that the ratio of $E_{nl(m-1)}^{(10\phi)} / E_{nlm}^{(10\phi)}$ is highest at equator, lowest at pole for all n and l (data not shown). And the ratio of $E_{nL(L-1)}^{(10\phi)} / E_{nLL}^{(10\phi)}$ always = 3 no matter what n it is. So $F_{\text{cntfgl-}\theta\phi}$ is the major driving force for pre-Sun disk-lyzation (and flattening). In comparison, at nLL = 322, the ratio of $E_{nL(L-1)}^{(1r)} / E_{nLL}^{(1r)} = -0.063 / (-0.095) = 0.66$ close to 1. Even more, the spin-perturbed $E_{nLL}^{(1r)}$ is directly additive to gravity's $E_n^{(0r)}$, where $|E_n^{(0r)}| \gg |E_{nLL}^{(1r)}|$. So $F_{\text{cntfgl-r}}$ only makes small contribution to the pre-Sun ball's disk-lyzation.
- 3) Similarly, the $n = 5$ (25×25) matrix can also be constructed for $\langle nl'm'|H_{1r}|nlm\rangle$ as in Table 4, and be analyzed as in Table 6. Due the length limitation of this paper, I am not going to present it here.

IV. It is mass occupancy that determines whether the out-shell of a pre-Sun ball goes to flatten or disk-lyzation

The best example is the Jupiter, which has a $p\{N, n=2..5/5\}$ QM structure (or $p\{N, n=1..4/5\}$ orbit, see my paper SunQM-1s3 and SunQM-3s2). $n/5$ means that base-pfactor- $n = 4*5^\wedge$. Jupiter's surface is set as $p\{0, 1\}$. The self-spin of Jupiter produced a reference-spin-frame, and provided the disk-lyzation force for each shell of $p\{N, n\}$ QM structure. In the inner shell of $p\{0, 1\}$ RF, which is $p\{-1, n=1..4\}$, the high mass density makes all $|nlm\rangle$ states are fully occupied by mass. So the disk-lyzation force of $F_{\text{cntfgl-}\theta\phi}$ and $F_{\text{cntfgl-r}}$ (plus un-discussed F_{cori}) is only able to flatten the Jupiter's surface, but not able to disk-lyze it. So Jupiter surface's flatten = 0.0649. However, for those shells outside of Jupiter surface $p\{0, 1\}$, including

$p\{0,n=1..4\}_o$, $\{1,n=1..4\}_o$, and beyond, they have very low mass density (because >99% of mass had fallen into $p\{0,1\}$ during collapse). So the disk-lyzation force of $F_{\text{cntf}gl-0\phi}$ (plus $F_{\text{cntf}gl-r}$ and F_{cori}) forces the residue mass to fill in the lowest energy nLL states, and this form the individual rings outside the Jupiter. The further accretion of mass in each ring forms the moons of Jupiter. So there should be a critical mass density (which is temperature dependent) to determine whether it is flattening or disk-lyzing.

To further illustrate the importance of the mass density in determine how much flatten of a planet/star, let us compare two gas planets: Jupiter and Saturn. Jupiter's flatten = 0.064 (spin period T = 9.925 hrs), Saturn's flatten = 0.098 (spin period T = 10.55 hrs). The question is why Saturn's flatten > Jupiter's? The larger flattening should be caused by either the larger r, or faster spin (= smaller spin-period). Jupiter's spin period is similar as (or a little bit faster than) that of Saturn's. If theirs mass densities were same, then due to it has a larger r, Jupiter should have larger flattening than that of Saturn. The only reason that Saturn's flatten > Jupiter's flatten is that Saturn has a lower mass density (or more accurately, lower mass occupancy) than that of Jupiter.

My best explanation is:

- 1) Jupiter's surface has a n shell of $p\{-1,5\}$ QM structure. Although from $p\{-1,4\}$ to $p\{-1,5\}$ is mainly made of n=4 orbit, but at the surface there is a thin layer of $|nlm\rangle=|54m\rangle$ QM state. (By my scientific reasoning) it has high mass occupancy (let us say ~90%) at n =5, l =4 sub-shell. And let us further assume (by my scientific reasoning) that in this l =4 sub-shell, the mass occupancy = 100%, 95%, 90%, 85% and 80% for states $|54\pm 4\rangle$, $|54\pm 3\rangle$, $|54\pm 2\rangle$, $|54\pm 1\rangle$, and $|540\rangle$. This is based on the nLL ($=|544\rangle$) has the lowest state energy, or the highest mass occupancy, and the total averaged mass occupancy for all m layers is 90%, so this $|54m\rangle$ sub-shell has a relative low flatten because its $m =0$ state (which correlate to the pole region of the $p\{-1,5\}$ RF ball) has close to full mass occupancy (=80%, close to 100%).
- 2) In comparison, Saturn's surface has $p\{-1,3\}$ QM structure. Although from $p\{-1,2\}$ to $p\{-1,3\}$ is mainly made of n=2 orbit, but at the surface there is a thin layer of $|nlm\rangle=|32m\rangle$ QM state. (Again by my scientific reasoning) it has much lower mass occupancy (let us say ~50%) at n =3, l =2 sub-shell. And let us further assume that in this l =2 sub-shell, the mass occupancy = 80%, 50%, 20%, for states $|32\pm 2\rangle$, $|32\pm 1\rangle$, $|320\rangle$, so this $|32m\rangle$ sub-shell has a relative high flatten because its $m =0$ state (which correlate to the pole region of the $p\{-1,3\}$ RF ball) has much less than the full mass occupancy (= 20%, << 100%). So mass occupancy (which equivalent to the mass density or the degenerate pressure of Pauli Exclusion Principle) does play a important role here.

For the Sun, the situation is complicated by the hydrogen fusion. We know that Sun surface has $\{0,2\}$ QM structure, though the main orbit is n=1, but top thin layer is at $|nlm\rangle=|21m\rangle$ QM state. (By my scientific reasoning) it has low (let us say ~50%) mass occupancy at n =2, l =1 sub-shell. Let us further assume (by my scientific reasoning) that in this l =1 sub-shell, the mass occupancy = 80%, and 20% for states $|21\pm 1\rangle$, and $|210\rangle$. So without H-fusion, the current Sun surface $\{0,2\}$ would have a very flattened shape, due to its pole region state $|210\rangle$ has very low (20%) mass occupancy. However, the heat of H-fusion excited the mass from lowest energy states $|2,1,\pm 1\rangle$ to the high energy state $|2,1,0\rangle$, make all three states almost evenly populated with mass (which equivalents to re-degenerate the three states of $|21m\rangle$). Meanwhile the high temperature generated extremely high thermal pressure to prevent the under-numbered mass in $\{0,2\}$ shell to collapse. So now the Sun's surface $\{0,2\}$ is almost perfectly spherical with flatten = $9E-6$. A second way of explanation: the % mass occupancy is temperature (or thermal pressure) dependent. At the cold-G, the mass in Sun's $\{0,1\}_o$ orbit is only ~ 50% mass occupancy, so it should be in oval shape. But at high temperature, the high thermal pressure decreases the mass capacity, now the mass occupancy becomes ~100%, so it becomes spherical shape.

However, for those shells outside of Sun surface $\{0,2\}$, including $\{0,3..6\}$, $\{1,2..6\}$, $\{2,2..6\}$ and beyond, they have very low mass density (because >99% of mass fell into $\{0,2\}$ during collapse). So the disk-lyzation force of $F_{\text{cntf}gl-0\phi}$ (and $F_{\text{cntf}gl-r}$ and F_{cori}) forces the residue mass to fill in the lowest energy nLL states, and this form the individual rings outside the Sun. The further accretion of mass in each ring forms the planet like Earth.

In summary (based on wiki "Degenerate matter" and added my $\{N,n\}$ QM theory), in the Solar $\{N,n\}$ QM, the $\{N,1\}$ RF pre-Sun ball is stabilized by the high % of mass occupancy and the high thermal pressure. In atom, the n shell is stabilized by the -/- electron repelling force in the same shell which against the +/- attraction force to the nuclei. In white dwarf, the $\{N,n\}$ shells is stabilized by the high % occupancy of electron and degeneracy pressure of electron. In neutron star,

the {N,n} shells is stabilized by the high % occupancy of neutron and degeneracy pressure of neutron. So the degenerate pressure and the thermal pressure are naturally unified for the function of preventing gravity collapse for a star, a pre-Sun ball, a white dwarf, a neutron star, and even an atom, and both pressures are mass density dependent (also see the discussion in paper SunQM-3).

V. Using the 1st order spin-perturbation result to explain celestial ball's flattening, disk-lyzation and ring structure

From Eq-24 and Eq-42, we know $B (= m * \omega_{1-spin}^2 * r_1^2) = 2A$. If we can combine Table 3e & 6d, then we can obtain the total spin-perturbed orbital energy change $\langle 3l'm'|H_{1r\theta\phi}|3lm\rangle$ for n =3 shell. After several tries, I realized that we cannot simply add Table 3e's result (in $\theta\phi$ -dimension) to Table 6d's result (in r-dimension) due to that they belong to two different dimensions. I guess that we can use the orthogonal vector adding method ($z^2 = x^2 + y^2$) to add them. I did not do it because of the unnecessary complication. Finally, even I guess it may not be right, I still use the simple addition of Table 3e to 6d to obtain Table 7, but name it as the combined spin-perturbed orbital energy (of $E_{nlm}^{(10\phi)}$ and $E_{nlm}^{(1r)}$, instead of total $E_{nlm}^{(1r\theta\phi)}$). The only purpose to construct Table 7 is to show that for almost all states (including |322>), the combined orbit-E are below zero, so spin stabilizes these orbital objects.

Table 7. The combined (not the total) spin-perturbed orbital energy ($E_{nlm}^{(1)}$), by simply add $E_{nlm}^{(10\phi)}$ in Table 3e to $E_{nlm}^{(1r)}$ in Table 6d. Unit = A ($= (1/2)m * \omega_{1-spin}^2 * r_1^2$).

$\langle 3l'm' H_{1\theta\phi} 3lm\rangle$	-0.93 300> + 0.37 320>	310>	311>	31-1>	0.37 300> + 0.93 320>	321>	32-1>	322>	32-2>
-0.93 300> + 0.37 320>	-0.123	0	0	0					
310>	0	-0.021	0	0					
311>	0	0	-0.156	0					
31-1>	0	0	0	-0.156					
0.37 300> + 0.93 320>					0.16 ?				
321>						-0.078			
32-1>							-0.078		
322>								-0.174	
32-2>									-0.174

Result and discussion (of Table 7):

1) As expected, the nLL effect is still valid for the combined $E_{nlm}^{(1)}$ (for n =3 shell as well as for all other n shells). For a ~100% mass occupied celestial body, this nLL effect causes the flatten of its spherical shape. For detailed study, please see paper SunQM-3s4. For a < 1% mass occupied orbital space, this nLL effect causes the disk-lyzation of a collapsed N super-shell. For detailed study, please see paper SunQM-3s2. For a < 1% mass occupied orbital space, this nLL effect also causes the ring structure (e.g., Saturn's ring). For detailed study, please see paper SunQM-3s4.

2) Combining Table 3e & 6d, the QM calculation reveals that Spin-frame does decrease the nLL orbit-E (in absolute value) than that of the non-spin frame (besides nLL has the lowest orbit-E among all nlm)! The combined $E_{nlm}^{(1)}$ matrix has negative diagonal elements. It means the spin perturbation stabilizes the orbital (planetary) objects. The unit $A = (1/2)m * \omega_{1-spin}^2 * r_1^2$ demonstrates that the higher the spin velocity (of the SunSpnFrm), the more stable effect the QM will provide. This provide the explanation (in paper SunQM-1s2 section VI) that it is unlikely for a non-spin star to generate (through quantum collapse of N super-shells) and maintain a planetary system. For a slow-spinning star, it can only generate and maintain a small planetary system (meaning planets are within {0,n=1..5}o super-shell). Only for fast-spinning (and large mass) star, it is possible to generate and maintain a large planetary system (like our Solar system with planets reach to {2,n=1..5}o, or even higher). Of cause, those captured planets are not included in this discussion. The same conclusion should also be valid for galaxies.

VI. Using the 1st order spin-perturbation result to explain the nL0 effect and the bipolar outflow

From Table 3e we can see that $m=0$ states of $|300\rangle$ and $|320\rangle$ are hybridized. It means that objects in $|300\rangle$ state is also automatically (and partially) in $|320\rangle$ state. The probability density of both $|Y(l=1,m=0)|^2$ and $|Y(l=2,m=0)|^2$ shows a bipolar extrude along z-axis (shown in Figure 3). This shape looks so similar to the shape of bipolar outflow that I believe it must have a cause-effect relationship.

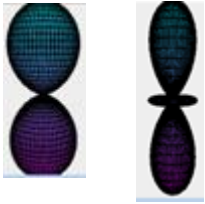


Figure 3. Probability density of $|Y(l=1,m=0)|^2$ (left), and $|Y(l=2,m=0)|^2$ (right), created by using online free software MathStudio (<http://mathstud.io>).

Now I can explain that how the bipolar outflow is formed in $\{N,n\}$ QM model for $n=3$ shell: From a particle QM view, before pre-Sun $\{N,n=2..6\}$ super-shell collapse, all objects in this super-shell are in RF movement. We know that those objects in $|nlm\rangle$ state with $m = +l$ have their L_z maximized and L_{xy} minimized. In contrast, those objects in $|nlm\rangle$ state with $m = 0$ have their L_z minimized and L_{xy} maximized. For a spinning pre-Sun ball, during collapsing of $\{N,n=2..6\}$ super-shell, only $< 1\%$ of objects (at the high end of Boltzmann velocity distribution) in each n shell will have high enough v (or equivalent to either high L_z , or high L_{xy}), to survive from the collapse. Those high L_z objects (they must have $L_{xy} \approx 0$) transform their RF heat (micro random) movement v into (non-random) macro movement orbit v in x-y plane, and re-gain the sustaining force (now it is $F = ma = mv_n^2/r_n$) to stay in the shell! This is equivalent to the spin-perturbation's nLL effect that fills some objects to the lowest orbital energy state at $|nLL\rangle$. On the other hand, those high L_{xy} objects (they must have $L_z \approx 0$) are forced to fill in to the highest orbital energy state (at $m=0$ of each l sub-shell, see Table 3e and 6d), So all maximum L_{xy} objects in $l=2$ sub-shell are forced to $|320\rangle$ state, all max L_{xy} objects in $l=1$ sub-shell are forced to $|310\rangle$ state, and all max L_{xy} objects in $l=0$ sub-shell forced to $|300\rangle$ state. Because $|300\rangle$ is hybridized with $|320\rangle$, so all max L_{xy} in $|300\rangle$ state are eventually go (or tunneling) to the even higher orbital energy $|320\rangle$ state. Therefore immediately after collapse, these objects still stay in orbit of $|320\rangle$ and $|310\rangle$, and have the probability density shape of $|Y_{20}|^2$ plus $|Y_{10}|^2$ (shown in Figure 3). In this way, these leftover objects in $|310\rangle$ and $|320\rangle$ states form the (apparently) bipolar outflow of $n=3$ shell (so bipolar leftover is more accurate than bipolar outflow in this situation). Because these $m=0$ states are the highest energy states, so objects in these states are only transient stable, they will be pull back to $\{N,1\}$ before too long. So the transient bipolar leftover looks like a burst of bipolar outflow! This is my explanation on how the (transient) bipolar outflow is formed (after collapse) using the $\{N,n\}$ QM model. Because this is a companion effect of nLL effect, and it is $m=0$, so I name it as "nL0 effect".

Of cause, the real situation is much more complicated. For example, in $n=5$ shell, besides $m=0$, most of $m=1$, $m=2$ states are also hybridized. However, the final result is the same: during collapsing, those maximum L_{xy} objects will move to the $m=0$ state (by tunneling through the hybridized states) and stay there transiently to become the (apparently a burst of) bipolar outflow.

Furthermore, my previous calculated spin-perturbation energy $\langle n'l'm' | \hat{H}_1 | nlm \rangle$ was forced to be within each n shell. In the real situation, $E_{n'l'm',nlm}^{(1)}$ may have some small contribution come from the hybridization of different n states. In this case, during collapse, the maximum L_{xy} ($m=0$, or m =small) objects at low n state may tunneling to high n states through the state-hybridization (e.g., $|210\rangle$ tunneling to $|320\rangle$, $|430\rangle$ or even higher n), and this forms the true bipolar outflow. I believe that this is how a black hole produces bipolar outflow when consuming a star (see paper SunQM-3s5). The Astrophysical jet can also be explained in this way once combined with the high-frequency multiplier n' theory (see paper SunQM-3s5).

VII. Construct a complete Solar system in r-dimension based purely on Schrodinger equation solution and {N,n} QM structure

Now let us build a complete (current) Solar system structure's probability density distribution in r-dimension based purely on solutions of Schrodinger equation we learned so far.

VII-a. Using solution of Schrodinger equation to construct a radial probability density distribution for super-shell space of $\{-1, n=1..6\}$

The super-shell space $\{-1, n=2..6\}$ is inside the Sun core $\{0,1\}$, so it is belong to the interior $\{N,n\}$, and they have orbit of $\{-1, n=1..5\}$. For orbital shell space $n=1$ of $\{-1,1\}$, majority of mass is in state of $|nlm\rangle=|100\rangle$. For simplicity, let us ignore the minority of mass that in states of $n \neq 1$ (due to high $n(s)$ have some residue $|\Psi|^2$ in $n=1$'s orbit space). The probability density distribution of mass is presented by the solution of Schrodinger equation $r^2 * |R(nl)|^2 * |Y(lm)|^2 * \sin(\theta) = |R(1,0)|^2 * |Y(0,0)|^2$. Its radial mass density distribution is expected to be similar as the single object's radial probability density distribution $r^2 * |R(1,0)|^2$.

For shell space $n=2$ of $\{-1,2\}$, majority of mass is in state of $|nlm\rangle=|2,0,1,m\rangle$. The small amount of mass that from states of $n \neq 2$ is also ignored. The probability density distribution of mass that presented by the solution of Schrodinger equation $r^2 * |R(nl)|^2 * |Y(lm)|^2 * \sin(\theta)$ is now composed by two of l sub-shells, $l=0$, and $l=1$. They are: $|R(2,0)|^2 * |Y(0,0)|^2$ and $|R(2,1)|^2 * |Y(1,m)|^2$. Similarly, the radial mass density distribution is $r^2 * |R(2,0)|^2$ and $r^2 * |R(2,1)|^2$. According to Figure 2a in paper SunQM-3, $l=0$ sub-shell is a little bit outside of $l=1$ sub-shell. According to section II & III, a SunSpnFrm causes $l=1$ sub-shell to have a lower state energy than that of $l=0$ sub-shell.

The same analysis for $n=2$ can be extended to $n=3, 4, 5$, and 6 . So now we have the QM state related mass density distribution along r for $\{-1, n=1..5\}$ orbits from the most inner to the outer as (Note: $r^2 * \sin(\theta)$ is omitted):

$$\begin{aligned} &|R(1,0)|^2 * |Y(0,0)|^2, \\ &|R(2,1)|^2 * |Y(1,m)|^2, |R(2,0)|^2 * |Y(0,0)|^2, \\ &|R(3,2)|^2 * |Y(2,m)|^2, |R(3,1)|^2 * |Y(1,m)|^2, |R(3,0)|^2 * |Y(0,0)|^2, \\ &|R(4,3)|^2 * |Y(3,m)|^2, |R(4,2)|^2 * |Y(2,m)|^2, |R(4,1)|^2 * |Y(1,m)|^2, |R(4,0)|^2 * |Y(0,0)|^2, \\ &|R(5,4)|^2 * |Y(4,m)|^2, |R(5,3)|^2 * |Y(3,m)|^2, |R(5,2)|^2 * |Y(2,m)|^2, |R(5,1)|^2 * |Y(1,m)|^2, |R(5,0)|^2 * |Y(0,0)|^2, \end{aligned}$$

Because these states are inside of Sun core $\{0,1\}$, so they have 100% mass occupancy for all orbits, so the lower state energy of nLL makes no practical difference for all l sub-shells, there are plenty of mass to fill all sub-shells. The lower state energy of nLL may flatten $\{-1, n=1..5\}$, but the effect is overcome by the heat generated from hydrogen fusion. As the result, the super-shell of $\{-1, n=2..6\}$ is almost perfectly spherical.

In this way, I have used the solution of Schrodinger equation to fill the mass into Sun's super-shell orbit space $\{-1, n=1..5\}$. The radial part is shown in Figure 4 as the curve of $\{-1, n=1..5\}$ Sun core.

VII-b. Construct a complete Sun ball by repeating the mass density distribution for super-shell of $N= -1, -2, -3, \dots$

Simply repeat section VII-a for the super-shell space of $\{-2, n=2..6\}$, and $\{-3, n=2..6\}$, ..., down to $\{-\infty, n\}$, or $r/r_1 = 0$. So we have a complete Sun core $\{0,1\}$ filled with mass which is based purely on the solution of Schrodinger equation. Figure 4 shows how to use Schrodinger equation's solution to construct the probability density for a Sun ball for two super-shell orbits from $\{N=-1, n=1..5\}$ to $\{N=-2, n=1..5\}$. It is done simply by taking the $N=-1$'s $\Sigma n=1..5$ curve, scale down r/r_1 to $1/36$ (because it is moved from $N=-1$ to $N=-2$ super-shell). You can add the probability density distribution of super-shell $N=-3$, or $N=-4$, to Figure 4, simply by taking the $\Sigma n=1..5$ curve, scale down r/r_1 to $1/36^2$, or $1/36^3$, then add to the Figure 4.

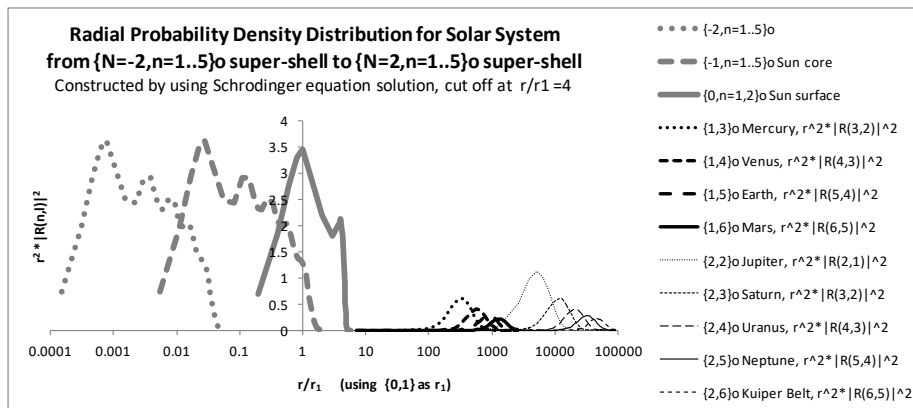


Figure 4. Using Schrodinger equation solution to construct the radial probability density distribution for Solar system for super-shells from $\{N=-2, n=1..5\}$ o to $\{N=2, n=1..5\}$ o. The $N=0$ super-shell cut-off at $r/r_1 = 4$.

Note-1: The intensities of $r^2 * |R(n,l)|^2$ in Figure 4 are not on scale between each N super-shell.

Note-2: in plot, $r_1=0.174$ with unit = E+9 meters.

Note-3: in the radial probability vs, r plot, only $r^2 * |R(n,l)|^2$ part is presented, the $|Y(l,m)|^2$ is omitted.

Note-4: the flattening effect is ignored in Figure 4 plot. If consider the flattening effect, then Figure 4 only (closely) presents the radial probability at $\theta = \pi/2$.

VII-c. For super-shell space of $N \geq 1$, or $\{1, n=2..6\}$ and beyond

The super-shell space of $\{1, n=2..6\}$ is also composed by many n shells and l sub-shells, and they can be listed (from inner to outer) in the same way as that in section VII-a. However, this super-shell is at outside of Sun, so it is belong to the exterior $\{N, n\}$. It has the mass occupancy $< 1\%$ for all possible orbital space, so only the lowest energy orbit nLL of each n shell is occupied by mass. Therefore, mass forms rings at nLL= 211, 322, 433, 544, and 655 in super-shell of $N=1$, which is equivalent to orbits in $\{N, n\}$ system as $\{1,2\}$, $\{1,3\}$, $\{1,4\}$, $\{1,5\}$, and $\{1,6\}$. Within hundreds of million years, the mass in these rings accreted into planets as we see today: Mercury at $\{1,3\}$ o, Venus at $\{1,4\}$ o, Earth at $\{1,5\}$ o, and Mars at $\{1,6\}$ o. I believe that the mass at orbit $\{1,2\}$ o was evaporated after Sun got matured and expand its rock-evap-line to $\{1,2\}$.

In this way, we have used the solution of Schrodinger equation to successfully build the planets in Sun's super-shell space $\{1, n=2..6\}$. By repeating this process, we can build the planets/belts for super-shell spaces $\{2, n=2..6\}$, $\{3, n=2..6\}$, and $\{4, n=2..6\}$. At shell space $\{4, n=4..6\}$, the strong interstellar wind overcome the weak disk-lyzation force by Sun's QM, so that the outer Oort cloud remains as more spherical rather than disk. Figure 4 shows the probability density up to $\{2,6\}$ o orbit.

VII-d. Shell space of $\{0,2\}$ and the shell space of $\{0, n=3..6\}$

The shell spaces of $\{0, n=3..6\}$ can be treated similarly as in section VII-c. Although the nLL still has the lowest orbit E, but due to the Sun's heat, the difference between E_{nLL} and other E_{nlm} getting smaller as orbit more close to the Sun. As the result, more mass will stay at state with $m \neq L$, so that the disk becomes more donut shape, or even more spherical, when n become really small. Again, I believe that the mass in shell spaces $\{0,3..6\}$ was evaporated after Sun got matured and expand its rock-evap-line to $\{1,2\}$. Although the Sun excites some mass from $\{0,2\}$ to the higher excitation states $\{0, n=3..6\}$ time upon time, most of this mass will transition back to the lower excitation state $\{0,2\}$ within hours. As the result, the Sun's corona in space $\{0, n=3..6\}$ has a spherical shape at $\{0,3\}$, and tend to be more flattened as n increases. The estimated $\Delta\theta'$ range of corona at each n shell is shown in Figure 2 of paper SunQM-1.

Sun's shell space of {0,2} is in a very unique situation: it is neither a complete interior {N,n} structure (which should be ~100% mass occupied), nor an exterior {N,n} structure (which should be <1% mass occupied). From wiki "Solar core", the Sun core (inside 0.20 of the solar radius) contains 34% of the Sun's mass, but only 0.8% of the Sun's volume. I guess that mass occupancy in shell space between {0,1} and {0,2} is no more than 50% of the total available (orbital) space. So as I have discussed before, hydrogen fusion's heat re-shapes a flattened Sun into to perfect sphere, and sustain this under-mass occupancy {0,2} QM structure with abnormal high thermal pressure.

In this way, we have constructed a complete Solar system structure based purely on solutions of Schrodinger equation (the wave function), and the Solar {N,n} QM structure, under a spinning SunSpnFrm. For a better understanding of the concept and process, please check two more examples in paper Solar-QM-p3s3, where I constructed Jupiter's (and Earth's) {N,n} QM ball by using the r-dimension probability, the {N,n} QM structure, and the mass occupancy, and then I used QM to explained the circulation pattern of their atmosphere.

Conclusion

- 1) A central G-force caused spherical spin frame theory is established, its $|\omega_n|$ value contour line is spherical shaped, and quantum decreases as r_n increases. Our pre-Sun ball's reference-spin-frame (SunSpnFrm) model is expected to be $\omega_{n-spin} = \omega_{1-spin} / n^x$, with $x \approx 3$.
- 2) The 1st order spin-perturbation problem has been solved for the spinning pre-Sun ball's {N,n} QM structure. The QM calculation shows that the spinning of Sun removes the degeneration of E_{nlm} , and causes nLL state (near equator) to be the lowest spin-perturbed orbit energy state among all nlm states. Therefore the nLL effect shows that the spin perturbation causes nLL orbit to have the highest probability density. Furthermore, the nLL effect is the driving force for the Sun's (and all other celestial bodies') flattening, disk-lyzation, ring formation. The nL0 effect (which is the companion effect of nLL effect) is the driving force for the bipolar outflow and astronomical jet.
- 3) It is mass occupancy that determines whether the outer shells of a pre-Sun ball goes to flattening or disk-lyzation.
- 4) A complete Solar system in r-dimension has been constructed solely based on {N,n} QM structure and solution of Schrodinger equation.

References

- [1] A series of my papers that to be published (together with current paper):
- SunQM-1: Quantum mechanics of the Solar system in a {N,n//6} QM structure.
 - SunQM-1s1: The dynamics of the quantum collapse (and quantum expansion) of Solar QM {N,n} structure.
 - SunQM-1s2: Comparing to other star-planet systems, our Solar system has a nearly perfect {N,n//6} QM structure.
 - SunQM-1s3: Applying {N,n} QM structure analysis to planets using exterior and interior {N,n} QM.
 - SunQM-2: Expanding QM from micro-world to macro-world: general Planck constant, H-C unit, H-quasi-constant, and the meaning of QM.
 - SunQM-3: Solving Schrodinger equation for Solar quantum mechanics {N,n} structure.
 - SunQM-3s1: Using 1st order spin-perturbation to solve Schrodinger equation for nLL effect and pre-Sun ball's disk-lyzation.
 - SunQM-3s2: Using {N,n} QM model to calculate out the snapshot pictures of a gradually disk-lyzing pre-Sun ball.
 - SunQM-3s3: Using QM calculation to explain the atmosphere band pattern on Jupiter (and Earth, Saturn, Sun)'s surface.
 - SunQM-3s6: Predict radial mass density distribution for Earth, planets, and Sun based on {N,n} QM probability distribution.
 - SunQM-5: C-QM (a new version of QM based on interior {N,n}, multiplier n' , $|R(n,1)|^2 |Y(l,m)|^2$ guided mass occupancy, and RF) and its application from string to universe.

SunQM-5s1: White dwarf, neutron star, and black hole re-analyzed by using C-QM.

[2] The citation of wiki "Solar core" means it is obtained from the Wikipedia online searching for "Solar core". Its website address is: https://en.wikipedia.org/wiki/Solar_core. This website address can be generalized for all other searching items.

[3] García, R. (2007) paper "Tracking solar gravity modes: the dynamics of the solar core", *Science*. 316 (5831): 1591–1593.

[4] Major QM books, data sources, software I used for this study are:

Douglas C. Giancoli, *Physics for Scientists & Engineers with Modern Physics*, 4th ed. 2009.

John S. Townsed, *A Modern Approach to Quantum Mechanics*, 2nd ed., 2012.

David J. Griffiths, *Introduction to Quantum Mechanics*, 2nd ed., 2015.

Stephen T. Thornton & Andrew Rex, *Modern Physics for scientists and engineers*, 3rd ed. 2006.

James Binney & David Skinner, *The Physics of Quantum Mechanics*, 1st ed. 2014.

Wikipedia at: <https://en.wikipedia.org/wiki/>

Online free software: WolframAlpha (<https://www.wolframalpha.com/>)

Online free software: MathStudio (<http://mathstud.io/>)

Free software: R

Microsoft Excel.

Public TV's space science related programs: PBS-NOVA, BBC-documentary, National Geographic-documentary, etc.

Journal: *Scientific American*.